2024-12

Studying the Effect of Bahir Dar Region Ionosphere on Gps Positioning During the Year 2015

Yitayew, Minyamr

STUDYING THE EFFECT OF BAHIR DAR REGION IONOSPHERE ON GPS POSITIONING DURING THE YEAR 2015

SUBMITTED IN PARTIAL FULFILLMENT OF THE
REQUIREMENTS FOR THE DEGREE OF
MASTER OF SCIENCE IN PHYSICS
AT
BAHIR DAR UNIVERSITY
BY

MINYAMR YITAYEW

DECEMBER, 2024
BAHIR DAR, ETHIOPIA

DECLARATION OF ORIGINALITY

I hereby declare that except where specific reference is made to the work of others, the content of this project are original and have not been submitted in whole or in part for consideration for any other degree or qualification in this, or any other university. This thesis work is my own work and contains nothing which is the outcome of work done, except as specified in the text and acknowledgments.

Minyamr Yitayew	_____	_____
Student name	Signature	Date
Melssew Nigussie (Ph.D)	_____	_____
Advisor Name	Signature	Date
Tamiru Nigussie (PhD)	_____	_____
Head of physics Department	Signature	Date

ADVISOR'S APPROVAL PAGE

To the best of my knowledge and as understood by the student in the research integrity and copyright disclaimer. This thesis entitled "STUDYING THE EFFECT OF BAHIR DAR REGION IONOSPHERE ON GPS POSITIONING DURING THE YEAR 2015" submitted in partial fulfillment of the requirement for the degree of Master of Science in physics adheres to the provision of guidelines, policies and legislations during his thesis and use of copyright material. The thesis is completed and can be presented to the thesis evaluation committee

_____	_____	_____
Name of Advisor	Signature	Date
(D/M/Y)G.C		

BAHIR DAR UNIVERSITY

COLLEGE OF SCIENCE

DEPARTMENT OF PHYSICS

The undersigned hereby certify that they have read and recommend to the faculty of graduate studies for acceptance a thesis entitled STUDYING THE EFFECT OF BAHIR DAR REGION IONOSPHERE ON GPS POSITIONING DURING THE YEAR 2015 in partial fulfillment of the requirements for the degree of Master of Science in physics (Space Physics).

Advisor:	Signature	Date
Melessew Nigussie (Ph.D.)	_____	_____
External Examiner:	Signature	Date
_____	_____	_____
Internal Examiner:	Signature	Date
_____	_____	_____
Chairman:	Signature	Date
_____	_____	_____

BAHIR DAR UNIVERSITY

Date: December, 2024

Author: Minyamr Yitayew

Title: Studying the effect of Bahir Dar region ionosphere on GPS positioning in 2015.

Department: Physics

Degree: MSc. Convocation: December Year: 2024

Permission is herewith granted to Bahir Dar University to circulate and to have copied for non-commercial purposes, at its discretion, the above title upon the request of individuals or institutions.

_____

Signature of Author

ACRONYMS

DAT----------Data Analysis Tool

DOD----------Department Of Defense

DOY----------Day Of Year

DPC----------Data Processing Core

ESA ----------European Space Agency

EUV----------Extreme Ultra Violet

GAGE -------- Group of Astronomy and Geomatics

GIM----------Global Ionospheric Maps

gLAB- --------GNSS-Lab Tool suite

GNSS----------Global Navigation Satellite System

GPS- ----------Global Positioning System

IONEX-------- Ionosphere Exchange

IPP----------Ionospheric Pierce Point

KML---------- Keyhole Markup Language

LT----------Local Time

NAV--------- ---Navigation

NEU---------- North, East, UP

Obs ----------observation

RINEX- -------Receiver Independent Exchange Format

RT----------Real Time

SP3----------Standard Product#3

TEC ----------Total Electron Content

UT ----------Universal Time

UV------ ----Ultra Violet

vTEC-------vertical Total Electron Content

DEDICATION

I would like to dedicate this work to my sister son Melese.

TABLE OF CONTENTS

Contents page

DECLARATION OF ORIGINALITY i
ADVISOR'S APPROVAL PAGE i
ACRONYMS iv
DEDICATION v
TABLE OF CONTENTS vi
LIST OF TABLE viii
LIST OF FIGURE ix
ACKNOWLEDGMENT x
ABSTRACT xi
CHAPTER ONE 1
INTRODUCTION 1
1.1 Background of the Study 1
1.2 The corrections of ionosphere effect 2
1.2 Motivation 4
1.3 Objectives of thesis 5
1.3.1 General Objective: 5
1.3.2 Specific Objectives: 5
1.4 Significant of the study 5
1.5 Organization of the thesis 6
CHAPTER TWO 7
LITERATURE REVIEW 7
2.1 IONOSPHERE 7
2.1.1 Structure of the Ionosphere 7
2.1.1.1 D-region 8
2.1.1.2 E-region 8
2.1.1.3 F-region 8
2.1.2 Variability of the ionosphere 11
2.1.2.1 Diurnal variation 11
2.1.2.2 Seasonal variation 12
2.1.2.3 Latitudinal variations 12
2.1.2.4 Geomagnetic activity and solar wind 12
2.1.2.5 Solar cycle variation 13
2.2 Global Positioning System (GPS) 13
2.2.1 GPS Signals 15
2.2.2 Function of GPS 15

2.2.3 GPS Navigation Message and segment 16
2.3 The Effects of the Ionosphere on the GPS Signals 16
2.4 Ionization profile of earth's upper atmosphere 19
2.5 Ionization rate 23
CHAPTER THREE 26
IONOSPHERIC MODEL AND gLAB SOFTWARE 26
3.1 gLAB software 26
3.1.1 General software characteristics 26
3.2 How gLAB mode work? 27
3.2.1 Positioning tab 29
3.2.2 Analysis tab 33
3.3 Ionosphere model 34
3.3.1 Klobuchar model 35
3.3.1.1 Klobuchar Algorithm Equations 37
3.3.2 BeiDou model 38
CHAPTER FOUR 41
DATA AND METHODS 41
4.1 Data 41
4.2 Methods 41
CHAPTER FIVE 43
RESULTS AND DISCUSSIONS 43
5.1 Daily positioning error commutation 43
5.2 Daily position estimation fluctuation 46
5.3 The monthly fluctuations in position estimation 49
5.4 Seasonal Positioning Estimation 53
CHAPTER SIX 56
CONCLUSIONS AND RECOMMENDATIONS 56
6.1 Conclusions 56
6.2 Recommendations 57
Bibliography 58

LIST OF TABLE

Table 4. 1: Station of study area.....41

Table 5. 1: horizontal and vertical maximum position error.....45

Table 5. 2: Monthly Fluctuations in Absolute Error. 52

Table 5. 3: Monthly Fluctuations in Root Mean Square Error. 52

LIST OF FIGURE

Figure 2. 1: *A typical electron density altitude profile and the various ionospheric regions (Hargreaves, 1992)* 10

Figure 2. 2: *Path of total electron content from satellite to receiver (J. Louis J. Ippolito, 2008)* 17

Figure 2. 3*: Signal affected at ionosphere region (Ledvina, 2004)* 18

Figure 2. 4: *Schematic diagram of an illustration of the geometry related to the solar irradiation (I) when penetrating a slab of thickness dz in the Earth's atmosphere at a Zenith angle (Brekke, 2013)* 20

Figure 2. 5**:** *Solar irradiation of intensity I decrease due to absorption downward in the Earth's atmosphere where the density increases towards the Earth.* 21

Figure 2. 6: *Chapman ionization profile for different zenith angles and maximum ionization production occurred when the sun is over head.* 25

Figure 3. 1: *gLAB GUI initial screen (Hernandez-Pajares, 2021)* 28

Figure 3. 2: *gLAB GUI initial Positioning tab (Segura, 2014).* 30

Figure 3. 3: *gLAB modeling tab (Klobuchar, 1988).* 31

Figure 3. 4: *gLAB filter tab (Klobuchar, 1988).* 31

Figure 3. 5: *gLAB GUI initial Analysis tab. (Segura, 2014)* 34

Figure 3. 6: *Klobuchar model layouts (Sanz, 2013)* 36

Figure 3. 7: *Ionospheric Pierce Point (IPP), vertical and slant delay illustration (Yilma, 2024)* 37

Figure 5. 1: NEU positioning error uncorrected on 01 April 2015 over Bahir Dar 43

Figure 5. 2: *NEU positioning error uncorrected, Klobuchar (GPS) model correction on 01 April 2015 over Bahir Dar* 44

Figure 5. 3: *NEU positioning error BeiDou model correction on 01 April 2015 over Bahir Dar* 44

Figure 5. 4: *x-y-z position estimation using uncorrected, Klobuchar model and BeiDou model correction on 01 April 2015 over Bahir Dar* 46

Figure 5. 5: *x-y-z position estimation using uncorrected, Klobuchar model and BeiDou model correction on 02 April 2015 over Bahir Dar* 47

Figure 5. 6: *x-y-z position estimation using uncorrected, Klobuchar model and BeiDou model correction on 03 April 2015 over Bahir Dar* 48

Figure 5. 7: *Monthly fluctuations in position estimation along the x-direction* 50

Figure 5. 8: *Monthly fluctuations in position estimation along the y-direction* 51

Figure 5. 9: *Monthly fluctuations in position estimation along the z-direction* 51

Figure 5. 10: *Seasonal Positioning Estimation along the x-direction* 54

Figure 5. 11: *Seasonal Positioning Estimation along the y-direction* 54

Figure 5. 12: *Seasonal Positioning Estimation along the z-direction* 55

ACKNOWLEDGMENT

First I would to say thank great thank you for Bahir Dar University department of physics and education of minister to planning and budgeting for any accesses to do so. Be following to this, I would like to say thank you for my advisor Melssew Nigussie (Ph.D) to advising properly and neatly to give positive attitude for me and also, his vast knowledge and experience in science will always remain with me as an example to follow. My adviser also announces new software which is called gLAB software. Finally I would to give a great thank you for my family and friends to give advice and support by different catalogs.

Minyamr Yitayew

Bahir Dar, Ethiopia

December, 2024

ABSTRACT

The thesis delves into an extensive analysis of the accuracy of position estimations through the utilization of Klobuchar model and BeiDou model corrections across varying time scales, encompassing daily, monthly, and seasonal fluctuations in 2015. We utilized gLAB as a tool to extract the position estimation with different corrections. The observation and navigation files of GPS observed over Bahir Dar, Ethiopia in 2015 have been used as input parameters for the execution of gLAB software. Notably, the Klobuchar model consistently exhibited superior performance compared to BeiDou model corrections on a daily basis, showcasing its enhanced ability to predict and adjust positional data accurately. This finding underscores the BeiDou model's precision and reliability in real-time positioning applications. Monthly assessments further reinforced the model's dominance in x, y, and z positioning estimations over GPS, yet the observed fluctuations in error rates from month to month suggest the influence of seasonal or environmental factors on the accuracy of these estimations. Factors such as solar activity, geomagnetic storms, and ionospheric variations were identified as key contributors to these fluctuations, emphasizing the necessity for vigilant monitoring and adjustments to ensure the precision of position calculations over extended periods. Moreover, the examination of seasonal position estimations revealed discernible trends in error rates, with peaks during equinoxes and reductions during solstices. Throughout these seasonal variations, the Klobuchar model consistently outperformed BeiDou model corrections, indicating its robust performance across different environmental conditions and time frames. The correlation between positioning errors and phenomena like neutral wind dynamics and ion accumulation dynamics further underscores the intricate interplay between environmental variables and positioning accuracy. The thesis accentuates the critical importance of acknowledging and accommodating the dynamic nature of position estimation accuracy across daily, monthly, and seasonal time scales. It highlights the complex interdependencies among ionospheric dynamics, geomagnetic activities, and environmental variables in shaping the reliability of positioning technologies. By recognizing the Klobuchar model’s consistent superiority in providing accurate estimations, the research underscores its potential to enhance the precision and dependability of satellite-based positioning systems. Continued exploration and research into these dynamic factors are deemed essential for the advancement of satellite navigation technologies and the refinement of position estimation methodologies in diverse and challenging environmental settings. This emphasis on ongoing investigation aims to deepen our understanding of satellite-based navigation systems, ultimately leading to improved accuracy and reliability in location determination processes across a variety of real-world scenarios.

CHAPTER ONE

INTRODUCTION

1.1 Background of the Study

The ionosphere derives its name from the term ion. High up in our atmosphere, roughly between 60 km and to 1000 km, counter regions of rarefied diffused gases. At these heights, the pressure is low enough that ions can be formed and travels freely for a considerable length of time without colliding and recombining into neutral atoms. At the outer reaches of the earth's environment, solar radiation strikes the atmosphere with a power density of 1370 Watts per square meter, a value known as the Solar Constant. This intense level of radiation is spread over a broad spectrum, ranging from radio frequencies through infrared, visible light, ultra violet, to X-rays. Cosmic rays and solar wind particles also play a role, but their effect is minor compared with the sun's electromagnetic radiation.

The ionosphere is defined as that part of the upper atmosphere where the density of free electrons and ions is high enough to influence the propagation of electromagnetic radio frequency waves (Parkinson and Spilker, 1996).

When a photon--radiated from the sun in the form of UV (Ultra Violet light), EUV (Extreme Ultra Violet light) or X-rays collides with an electron gyrating around an atom of the rarefied gas, there is a great possibility that the electron will change its course and come loose from the atom. The free negatively charged electron exists on its own for some time and leaves behind a positively charged atomic part, called an ion. After some time the free electron can recombine with an ion and form again a neutral atom (or even a negative charged ion). This process is called recombination.

The ionosphere is a 90-mile (150-km) thick layer of the upper atmosphere in which ultraviolet radiation from the sun has ionized a fraction of the gas molecules, thereby releasing free electrons (ions). The shape of the ionosphere and its electron density varies with latitude, time of day, time of year, number of sunspots, solar flares, and other cosmic activity.

Different layers of rarefied gases at different heights and with different ionization densities. As we noted earlier, it is the radiation of the sun that causes the ionization. So the sun is the prime motor that drives the whole process. Therefore, solar conditions will be of great importance to the propagation factors. Derived from the sun's leading role and influenced by the ionization capabilities of the rarified gasses, ionization density is strongly dependent on whether it is day and night, what time of the day or night it is, whether it is winter and

summer (season of the year), and the specific location, (longitude and latitude). Location means how close to or far away from one is from the equator. In turn, location also determines if it have longer or shorter daytime and nighttime, in contrast to more or less equal daytime and nighttime near the equator. In other words, can divide the main phenomena into the following categories such as diurnal, seasonal, geographical and geomagnetic activity.

1.2 The corrections of ionosphere effect

The different methods can be adopted to minimize the ionosphere effect:

- use of dual-frequency technique,
- use of ionospheric model.

The quality of GNSS operations are affected by different errors depending on three major error sources; satellite dependent errors, such as (satellite clock error and satellite orbital error), receiver dependent errors such as (antenna phase center variations and receiver clock error), and signal path dependent errors such as (cycle slip, multipath, tropospheric error and ionospheric error). The ionospheric delay is the current major source of range delay faced by single-frequency GNSS observations (Kunches and Klobuchar, 2001). The applied ionospheric delay mitigation technique depends on the type of collected observations. Since the ionospheric delay is depending on the signal's frequency, so users of dual-frequency receivers can eliminate the first-order term of the ionosphere delay by a combination of dual frequency observations. Users of single frequency receivers must use differential or ionospheric correction model. The ionospheric delay is also dependent on the activity of the sun which is varying during the day time and follows a cycle of about eleven years. The ionospheric delay varies according to the solar activity and other natural phenomena in the ionosphere as well as the frequency of the propagated signal. For mid-latitudes regions, GPS L1 pseudo-range is faced by an ionospheric zenith ranging delay of about 5–15 m on daytime, and 3 m in the evening. As the ionospheric activity is highly variable, so at the peak of solar activity the ionospheric delay can be up to hundreds of meters. Different models are used to eliminate the ionospheric error for single-frequency GNSS users. GPS system users use the Klobuchar model (Klobuchar, 1982) to mitigate the ionospheric delay. GPS control segment broadcasts eight parameters for Klobuchar model based on seasonal ionospheric variations and average solar flux, so the correction accuracy is about 50-60 % (Kunches and Klobuchar, 2001). BeiDou system broadcasts also eight parameters for Klobuchar model based on continuous monitoring stations under the geographic coordinate system. The ionospheric delay of satellite-station direction can be identified using of dual-frequency

pseudoranges. Satellite and receiver hardware delay can be deducted in combination observations. Through projection function, the Vertical Total Electron Content (vTEC) of corresponding puncture point can be evaluated. The eight parameters can be evaluated with the vTEC as model observables, and broadcast to BeiDou users.

The electron density distribution over this region is, therefore, very crucial for satellite communication and navigation systems. However, the distribution of these electrons over the ionosphere exhibits complicated structure especially during increased solar activity. Hence, exploring the ionosphere is of utmost interest due to the complexities associated with the region (Tsurutani, 2000; YU *et al*., 2009; Michael, 2009). Nowadays, several ionospheric delay models can be used for real-time or post processed applications. Among these ionospheric delay models, the Klobuchar model, which is driven by broadcast ephemeris, is widely used by GPS users (Ke Su *et al*., 2019; Klobuchar, 1987).

Ionospheric correction refers to the techniques used to mitigate the effects of the ionosphere on radio signals, particularly for navigation systems like GPS and for communication technologies. Here are the main approaches to achieve ionospheric effect correction:

Total Electron Content (TEC) is a key parameter that represents the total number of electrons along a path between a transmitter and receiver. Corrections can be made based on TEC values for specific frequencies. Delay Estimation, TEC values help estimate the ionospheric delay for GNSS signals. By knowing the TEC along the signal path, corrections can be applied to improve the accuracy of the positioning solution Mapping and Modeling, TEC data is also used to create ionospheric maps, which provide insights into the electron density distribution and help refine correction algorithms. Pseudorange Measurements, calculate TEC for each GNSS satellite signal received at the ground stations. This involves analyzing the phase shift and time delay experienced by the signals as they pass through the ionosphere. In addition to pseudorange, the carrier phase of the GNSS signal can be measured. This measurement is more precise and is used for high-accuracy TEC estimation. In addition to pseudorange, the carrier phase of the GNSS signal can be measured. This measurement is more precise and is used for high-accuracy TEC estimation. The ionospheric delay can be estimated using the difference between the pseudorange and carrier phase measurements at the two frequencies. The ionospheric delay (in meters) can be expressed as:

$$I(s, t) = \frac{40.3}{f^2}TEC(s,t) \qquad (1.1)$$

Where, t is the time of an epoch, f is the frequency of the propagated signal, and s is the number that defines the satellite PseudoRandom Noise (PRN) codes.

Frequency Scaling, the ionosphere is a dispersive medium, thus a linear combination of observable on the two frequencies is needed to remove this effect for positioning (Misganaw, 2017). Corrections can be applied using a frequency scaling factor derived from the characteristics of the ionosphere. This often involves using the standard model predictions and adjusting them for the actual frequency of the signals being used.

Phase and Group Delay Corrections, these corrections are applied to account for the time delay experienced by signals traveling through the ionosphere at different frequencies.

Real-time Monitoring Networks

Ground Stations, networks of ground-based stations continuously monitor ionospheric conditions and provide data that can be used to adjust signal processing in real time. Satellites, some satellites are equipped with instruments to measure ionospheric effects directly.

1.2 Motivation

A notable gap persists in research focusing on positioning estimation challenges and opportunities in Bahir Dar, a region with unique environmental conditions that can significantly affect the performance of GPS-based systems. Region like Amhara, located in Ethiopia, present a complex terrain characterized by diverse topography, ionospheric disturbances, and geomagnetic variability, posing distinct challenges for achieving accurate position estimations. Understanding the intricate interplay of these factors is essential for enhancing location tracking technologies in Ethiopia specially Bahir Dar, and addressing the specific positioning system challenges prevalent in the broader East African context.

This study seeks to fill the aforementioned research gap by delving into the nuances of accuracy fluctuations in positioning estimations across varying timeframes in Ethiopia, with a specific emphasis on Bahir Dar. By scrutinizing the performance disparities between GPS data and model-based corrections in this region, the research aims to illuminate the specific obstacles and possibilities for improving positioning accuracy in Bahir Dar. Through a detailed analysis of how ionospheric and geomagnetic variations impact positioning precision along different axes, valuable insights can be gained to enhance the reliability of satellite-based positioning systems in Bahir Dar and its neighboring region.

The investigation into the influence of environmental dynamics on positioning accuracy in Bahir Dar holds significant implications for the region's development across sectors such as transportation, agriculture, telecommunications, and defense. By uncovering the specific challenges posed by Bahir Dar unique topographical and atmospheric conditions, this research not only addresses a critical knowledge gap but also paves the way for

tailored solutions to enhance location tracking technologies in Bahir Dar. Ultimately, the findings of this study are expected to contribute to the advancement of positioning technologies in Bahir Dar, aligning with global efforts to elevate the precision and dependability of location tracking systems worldwide.

1.3 Objectives of thesis

1.3.1 General Objective:

To understand the effect of the Bahir Dar region ionosphere on the GPS positioning during the year 2015.

1.3.2 Specific Objectives:

1. To analyze the performance differences between GPS based data on Klobuchar and BeiDou model-based corrections in positioning estimations over Bahir Dar.
2. To understand the diurnal, monthly, and seasonal variations of the GPS positioning estimation fluctuation over Bahir Dar.

1.4 Significant of the study

The Klobuchar model is the standard ionospheric correction algorithm implemented in the GPS system, and its performance is crucial for improving the positioning accuracy of single-frequency GPS receivers in regions like Bahir Dar. However, the effectiveness of the Klobuchar model can be limited in areas with high ionospheric variability, necessitating the need for a comprehensive evaluation of its performance.

This study aims to assess the ability of the Klobuchar ionospheric correction model, implemented using the gLAB software, to improve the positioning accuracy of single-frequency GPS receivers over the Bahir Dar region in Ethiopia during the year 2015.

By quantifying the reduction in horizontal and vertical positioning errors achieved through the application of the Klobuchar correction, this research will contribute to a better understanding of the ionospheric effects on single-frequency GPS positioning in the equatorial and low-latitude regions of Ethiopia. The findings can guide the optimization of GNSS-based services and applications, such as navigation, surveying, and location-based services, in the Bahir Dar region and similar ionospherically challenging areas.

Furthermore, the insights gained from this study may also inform the development of more advanced ionospheric correction techniques, potentially involving the integration of regional or global ionosphere models, to further enhance the positioning accuracy of single-frequency GNSS receivers in the study area and beyond. Geophysical Insights that understanding the ionosphere's behavior in a specific region helps researchers grasp its impact on global positioning systems, particularly in areas with limited existing data. By analyzing

ionospheric variations, the thesis can contribute to developing models that enhance the accuracy of GPS readings, crucial for various applications like navigation, surveying, and disaster management. Bahir Dar's unique geographical and environmental conditions provide a valuable case study. Insights gained can be applied to improve local navigation and geo location services. The research can also shed light on how space weather events affect the ionosphere, contributing to broader studies on climate and atmospheric science. Findings could inform the development of new technologies or methodologies for mitigating ionospheric interference, benefiting sectors reliant on precise GPS data.

1.5 Organization of the thesis

This thesis contains six chapters; chapters one includes: background of study, statement of the problem, general and specific objectives, significance of the study and; chapter two includes: literature review, Structure of the ionosphere, effects of ionosphere on GPS signal, , variability of ionosphere and ionization rate and earth profile, GPS, GPS signal, Function of GPS, chapter three includes; ionospheric model, gLAB software,; chapter four includes: data set and methodology; chapter five includes; result, discussion and chapter six includes; conclusion and recommendation.

CHAPTER TWO

LITERATURE REVIEW

2.1 IONOSPHERE

Ionization is a phenomenon in which an electrically neutral atom either gains or loses an electron, resulting in a net charge. In the upper atmosphere, high-energy photons from the sun collide with gas molecules, stripping them of electrons and thus ionizing them. Photoionization, or ionization due to electromagnetic waves, can be represented mathematically by the equation:

$$A + \frac{hc}{\lambda} \rightarrow p + e^{-} \qquad (2.1)$$

Where

A is some arbitrary neutral atom,

hc/λ is the energy of an incident photon of wavelength ,

p is a positive ion, and

e^{-} is an electron.

This process can only occur if the photon energy exceeds the ionization energy E ion.

The troposphere is the dense, humid layer of the atmosphere near the surface of the Earth. This layer refracts the satellite signals in proportion to the humidity and density of the air. The ionosphere has been extensively studied in terms of the physical and chemical processes in it. The different constituents of the neutral atmosphere with their ionization energy, the Earth's magnetic field which embeds the region and the different activities observed in the Sun all contribute to characterizing the ionosphere.

2.1.1 Structure of the Ionosphere

The sun radiates sufficient energy at short wavelengths that can drive the photoionization process. This process at high altitudes in the Earth's atmosphere results in a partially ionized region called the ionosphere. Due to the height dependence of solar energy absorption, physics of recombination and composition of the atmosphere, there are different ionospheric regions. These regions have their own associated different physical processes and all correspond to different altitude and electron density levels. These ionospheric regions are named D (at about altitude between 60 km-90 km), E (90 km- 150 km) and F (> 150 km). D and F regions are extensions of E, which was discovered first. The F region can be separated into two regions: F1 and F2 during the daytime. It merges at night to form a single F region.

2.1.1.1 D-region

The D region is the lowest at altitudes between 60- 90km where the atmosphere is comparatively dense. It is produced by hard X-rays from the Sun during the daytime and quickly disappears at night. The D region is very weakly ionized, highly collision, primarily composed of molecular oxygen ions (O^{+2}) and nitric oxide ions (NO^{+}), ionization results mostly from photoionization of NO by Lyman-α radiation (121.6nm) and a molecular O_2, N_2, and NO. Since the air density is still relatively high at this latitude, the ions and electrons present can easily recombine, resulting in a strong diurnal variation in electron density in the D region (Hunsucker and Hargreaves, 2007). During the day, some reflection can be obtained from the D field, but the frequency of radio waves is reduced this is the cause of the marked reduction in the range of radio transmissions in the daytime.

2.1.1.2 E-region

Below the F region is the E layer produced by ionization of molecular and atomic oxygen and molecular nitrogen by soft X-ray and Lyman -αradiation (102.6 nm). It ranges from about 90 km to 150 km (Hunsucker and Hargreaves, 2007) and is present throughout the day with a much-reduced electron density at night. This layer is present by day and decreases by night. Its shape is only a simple in flexion in the profile, but a valley usually appears thus marking a local maximum. The production processes in the E region are very complex since electrons and ions recombine quite quickly here, ionization levels drop rapidly after sunset and the E layer almost vanishes during the night(McNamara, 1991). An additional feature of this region the appearance of its transient character is called the sporadic E layer (Es layer), a thin layer that same time shows large enhancements of electron density and is associated with quasi -periodic amplitude scintillations (Gaussiran e*t al.*, 1995).

2.1.1.3 F-region

The F-layer is the most prominent layer of the ionosphere, containing the majority of the electron content and is ionized by ultraviolet and extreme ultraviolet radiation. This layer extends from about 150 kilometers above the Earth's surface to about 1000km (Rishbeth and Garriott, 1969). The F region is the most critical layer for long-distance communication and it often splits into F1 and F2 sub-regions throughout the day. The F1 region is located approximately 150-210km above the Earth’s surface, which exists only during daytime and can be distinguishable as an flexion in the profile. When it is present, it changes rapidly in a matter of minutes. It is more pronounced during the summer than during the winter months for low solar sunspot numbers and for periods with ionospheric storms. The ionization at this region is caused by the absorption of EUV radiation and by

the molecular species ($O^{+,}$ N^{+2}). The electron densities are largely derived from the Sun's zenith angle, which accounts for day experienced by GPS and the most abundant ion in this area is atomic oxygen(Chapman ,1931).The F2 region is located approximately 210-1000km above the Earth's surface which contains the maximum of the electron density profile and is predominantly populated with oxygen ions (O^{+}). The maximum electron density is typically 10^{6} electrons per cubic centimeter (Hunsucker and Hargreaves, 2007).The ionization of oxygen and molecular nitrogen by extreme ultraviolet radiation(EUV) is the primary cause of the F2 region. Although it does not disappear during nighttime, the electron density during this period decreases by about one order of magnitude. It is also very sensitive to the sun spot cycle. The region below the F2 region (D, E, F1) is referred to as the bottom side of the ionosphere, whereas the region above is referred to as the topside.

Typical vertical structure of the ionosphere based on electron density is shown in Figure 2.1. As one goes to a high altitude the electron concentration increases till the F region peak electron concentration. After this peak the concentration decreases monotonically. The figure also shows the day and night time electron density variations associated with solar cycle. Unlike the night time and at solar minimum, the electron density is maximum during day time and solar maximum. Not only the electron density decreases at night but the F1 and D regions disappear after sunset. This is due to recombination process which is dominant during the night time (Hargreaves, 1992).

Unlike the solar radiation the density of neutral particles decreases with altitude. As a result, there has to be a maximum ionization. This can be explained by following the radiation from the sun. When it first reaches rarefied topside atmosphere it encounters and ionizes the few number of particles. Then it goes deep down, where dense particles are found but through the way energy is lost during ionization, so there must be a height where moderate number of particles and ionization energy are available to produce maximum ionization (Chapman, 1931).

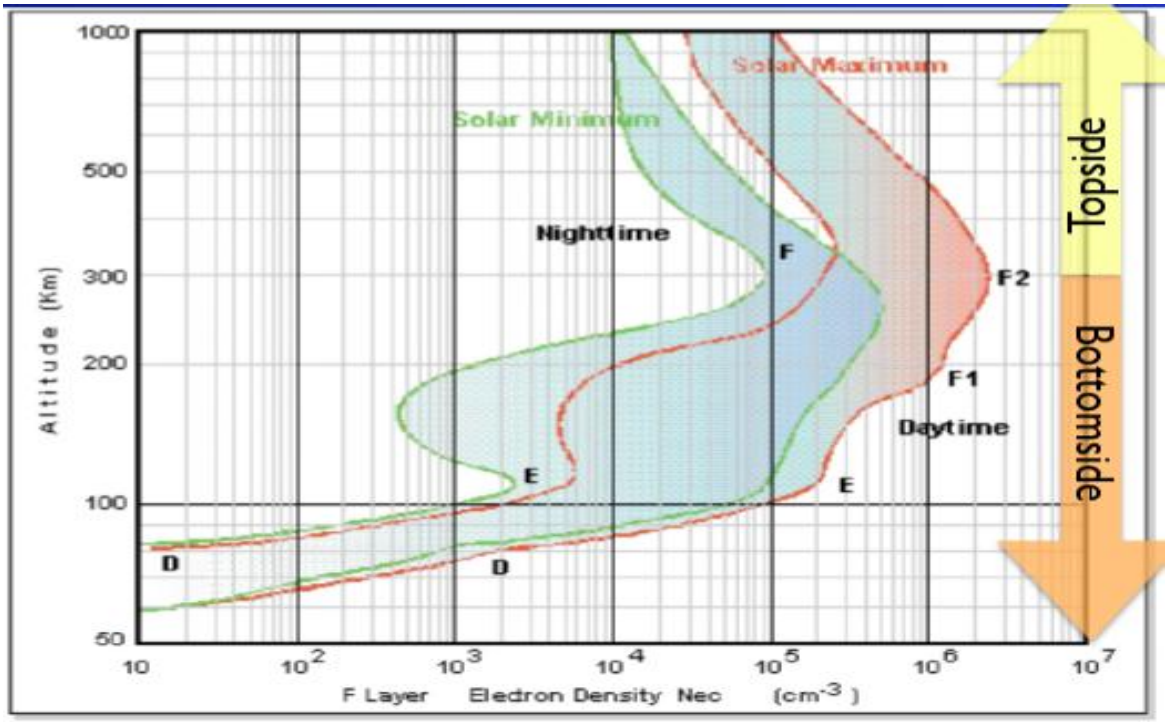

Figure 2.1: *A typical electron density altitude profile and the various ionospheric regions (Hargreaves, 1992)*

The ionosphere is the densest plasma between the Earth and Sun, and is traditionally believed to be mainly influenced by forcing from above (solar radiation, solar wind magnetosphere).

There are two ways to compensate for the atmospheric delays: modeling and direct measurement. The ionospheric and tropospheric delays are inversely proportional to the square of the frequency. If a receiver can receive L1 and L2 frequencies, it can measure the difference between the two signals and calculate the exact atmospheric delay. Most receivers currently use mathematical models to approximate the atmospheric delay.

The ionosphere is a partially ionized region of the earth's upper atmosphere. It comprises of free electrons and ions, generally in equal numbers, in a medium that is electrically neutral (Ioannides *et al.*, 2000). The ionosphere extends approximately from about 60 to 1000 km. The main sources of ionization are the solar radiations such as extreme ultra violet (EUV) and X-ray radiations. Apart from photoionization, ionization by collisions of energetic particles due to particle precipitation from the magnetosphere at the aurora latitudes is another source of ionization at the topside ionosphere (Kelley *et al.*, 1996). The processes explained above lead to the production of plasma which undergoes chemical reactions with the neutrals, diffuses due to the gravitational force and pressure gradients, and it is transported through neutral winds and electric field under the influence of the earth's

magnetic field. The ionosphere is a highly variable and complex physical system where ions and electrons are present in quantities sufficient to affect the propagation of radio waves (Matsushita and Campbell, 1967). Free electrons populating this region of the atmosphere affect the propagation of the radio signals, changing their speed and direction of travel. Hence, the accumulation of electrons affects the electromagnetic waves that pass through the ionosphere by inducing an additional transmission time delay (Klobuchar *et al*., 1996). This delay is directly proportional to the number of free electrons in a cylinder of unit cross-section along the signal path extending from the satellite to the receiver on the ground and inversely proportional to the square of the frequency of the trans-Ionospheric radio wave (Hofmann-Wellenhof *et al*., 1992). Due to the unique geometry of the magnetic field, these phenomena are most pronounced in low-latitude and equatorial regions such as Ethiopia. In such regions, the plasma density in the ionosphere shows significant variations with time of day, latitude, longitude, season, and solar and geomagnetic activity, which can result in a variation of different parameters such as total electron content (TEC).

The presence of ions and free electrons decreases above 1,000 km, although traces of free electrons are present up to altitudes of a few tens of thousands of kilometers in the plasma sphere or proton sphere (named after the H^+ ions predominant in this region (Davies, 1990).

2.1.2 Variability of the ionosphere

The Sun and its activities are the main source of ionization of the ionosphere (Carpenter, 2004). The existence of free electrons and the ionosphere shows a wide range of spatial and temporal variability of electron density, ranging from small fluctuations to large changes. The ionospheric structure and the temporal variation of the Earth-Sun geometry is related to the Earths daily rotation and yearly revolution and the electron density distribution varies considerably with time (diurnally, seasonally), space (geographic location), Suns activity (sunspot cycle) and with other solar-related ionospheric and geomagnetic disturbances.

The ionosphere varies greatly because of changes in the two sources of ionization and because it responds to changes in the neutral part of the upper atmosphere in which it is embedded. This region of the atmosphere is known as the thermosphere. Since it responds to solar EUV radiation, the ionosphere varies over the 24-hour period between daytime and nighttime and over the 11-year cycle of solar activity.

2.1.2.1 Diurnal variation

Due to the earth rotation, the relative position of the Sun and Earth changes with time, following a daily cycle. As the Earth rotates with respect to the Sun, the intensity of the solar radiation increases and the ionization also increases to a maximum at around noon. Because

of the Earth's rotation around the Sun, the density of electrons varies from day to night (Chapman, 1931). The Sun's large EUV and X-ray radiations cause a higher electron density during the day than at night, when photo-ionization is absent (Chapman, 1931; Rishbeth and Garriott, 1969; Kelley, 2009).

2.1.2.2 Seasonal variation

Due to shifting orientation of the Sun with respect to the Earth's axis, high electron density values are usually seen during the equinoctial months (March and September) and in summer, although low values are seen in winter (Chapman, 1931). As the Earth revolves around the Sun, a seasonal cycle is generated and determined by which hemisphere the Sun is overhead. It is summer on the hemisphere where the Sun is overhead and winter on the other hemisphere. During solar cycle 23 (Lee *et al*., 2004) analyzed the seasonal anomaly, which occurs mostly at mid-latitudes and is more apparent in the northern hemisphere than in the southern hemisphere. The Sun is overhead at the equator around the time of the equinoxes. Seasonal variation influences animal anatomy, such as body size or fat layers (Heldmaier et al., 1981; Aars and Ims, 2002), physiology, such as hormone secretion, and human actions (Romero, 2002). Changes in photo period can cause seasonal adaptations, which are mediated by neuroendocrinology (Goldman, 2001).

2.1.2.3 Latitudinal variations

The diurnal and seasonal behaviors observed the Suns position relative to the atmosphere plays significant role in latitudinal variation in the ionospheric electron density because the solar zenith angle (χ) measured from the observers local vertical to the Sun determines the intensity of ionization. Over the equator the ionospheric densities are expected to be higher compared to other geographic locations. Solar radiation enters the atmosphere at an oblique angle as latitude increases on either side of the geographic equator, resulting in lower ionospheric concentrations (Merwe, 2011).

2.1.2.4 Geomagnetic activity and solar wind

Geomagnetic activity, like sunspot flares, radio flux, and flares and CMEs, has solar cycle reliance, but it's more complex. There are a number of indices of geomagnetic activity; most measure rapid (hour-to-hour) changes in the strength and/or direction of Earth's magnetic field from small networks of ground-based observatories. The majority of geomagnetic activity indices use tiny networks of ground-based observatories to measure rapid (hour-to-hour) variations in the strength and/or direction of Earth's magnetic field. Solar wind is a flow of ionized plasma and solar magnetic field that provides interplanetary space. It is the result of huge difference in gas pressure; this pressure difference drives the plasma out ward.

Solar wind is significantly influenced by solar activity and interact with the magnetic field of the Earth. It consists largely of ionized hydrogen, ionized helium still fewer ions of heaver elements. The quiet sun does not only radiate electromagnetic waves in the frequency range from a few nanometers to a few hundred meters, but also particles. This wind is not a steady wind, but varies quite strongly in velocity as well as density at a distance from the sun corresponding to the Earth's orbit. During the quite condition the wind has a medium velocity of 400 km/s and can however, vary between 200 and 700 km/s. The wind contains plasma with very high thermal energy and magnetic field with it (Nuru, 2019).

2.1.2.5 Solar cycle variation

Measurements of the sunspot number, an indicator of solar activity, show that the sun goes through a periodic rise and fall in activity with a period of about 11 years. Since ionization is driven by solar electromagnetic and corpuscular radiation, it is a function of solar activity. At solar maximum the sun emits more radiation and therefore ionization is greater. Thus the critical frequencies of the ionospheric layers are greater during high solar activity periods (Merwe, 2011).

2.2 Global Positioning System (GPS)

GPS is a positioning system based on a network of satellites that continuously transmit coded information. The information transmitted from the satellites can be interpreted by receivers to precisely identify locations on earth by measuring distances from the satellites.

Global Navigation Satellite Systems (GNSS), such as the Global Positioning System (GPS), have become ubiquitous in various applications, ranging from navigation and surveying to scientific research and emergency response. However, the performance of GNSS-based positioning can be significantly degraded in regions with high ionospheric activity, such as the equatorial and low-latitude areas near the geomagnetic equator.

The Bahir Dar region in northern Ethiopia is located within this ionospherically challenging environment, where the ionosphere can introduce significant delays and distortions in GNSS signal propagation, leading to substantial positioning errors. This is particularly problematic for single-frequency GNSS receivers, which are widely used in many cost-sensitive applications, as they rely on simplified ionospheric correction models to compensate for the ionospheric effects.

Precisely identify locations on earth by measuring distances from the satellites. The GPS signal communicates information about the precise position of the satellite and the precise time of the signal. Each satellite orbits the earth in about 12 hours. The satellite orbits repeat roughly the same ground track each day A GPS receiver is able to trilateration its own

position on the surface of the Earth by calculating its distance from several satellites. This is accomplished by sending a signal from the satellite to the receiver and keeping track of the amount of time the signal took to travel between the two. Signals are sent in the form of radio waves, which travel at the speed of light, c, in a vacuum. Therefore, the receiver simply multiplies the travel time of a given signal by c to estimate the distance it traveled. The electron density distribution over this region is, therefore, very crucial for satellite. Global studies in positioning estimation have extensively explored the critical role of accurate positioning systems across diverse sectors in regions such as the Americas, Asia, and Africa.

However, the distribution of these electrons over the ionosphere exhibits complicated structure especially during increased solar activity. Hence, exploring the ionosphere is of utmost interest due to the complexities associated with the region (Tsurutani, 2000; YU *et al*., 2009; Michael, 2009). Nowadays, several ionospheric delay models can be used for real-time or post processed applications. Among these ionospheric delay models, the Klobuchar model, which is driven by broadcast ephemeris, is widely used by GPS users (Ke Su *et al*., 2019).

The computation of reliable vertical total electron content (vTEC) of the ionosphere is at the same time useful and challenging goal. Useful: because in both Science and Technology fields, they can provide valuable information concerning Space Weather Events.

Unfortunately, GPS signals must propagate through Earth's atmosphere to reach a receiver. A number of propagation effects cause the signal to travel differently than it would in a vacuum, making the receiver's estimate of its position very poor. The discrepancy between the estimated position and the true position is termed GPS positioning error.

Fortunately, through careful analytical study, relevant atmospheric propagation effects have been identified and quantified. Further, computational models of these effects have been developed, allowing GPS receivers to obtain real-time estimates of positioning error and compensate for its effect when calculating their position.

Each GPS satellite transmits data that indicates its location and the current time. All GPS satellites synchronize operations so that these repeating signals are transmitted at the same instant. Satellite deployment started at the end of the1970s and reached Full Operational Capability (FOC) in July 1995 (Sanz *et al*., 2013).

Regarding satellite positioning, the ionosphere is one of the main error sources in signal propagation. The range of the ionospheric error is proportional to the Total Electron Content (TEC) along the signal path, which varies depending on observation latitude, local time, season, geomagnetic activity, solar cycle, and other anomalies and irregularities (Seeber,

2003). Different methods can be adopted to minimize the ionospheric effect in positioning, such as the use of an ionospheric model. Models using ionospheric parameters broadcasted within navigation messages have been widely used to minimize the ionospheric effect on signal propagation for users of single frequency receivers. (Klobuchar, 1987) developed the first algorithm for ionospheric correction in the mid1970s for GPS single frequency users.

2.2.1 GPS Signals

Legacy GPS signals are transmitted on two radio frequencies in the L band, referred to as Link 1 (L1) and Link 2 (L2), or L1 and L2 bands. They are right-hand circularly polarized and their frequencies are derived from a fundamental frequency f_0 = 10:23 MHz, generated by on board atomic clocks.

L1 = 154 x10.23MHz = 1 575.420MHz $\Rightarrow \lambda L1 = 19.0$ cm

L2 = 120 x 10.23MHz = 1 227.600MHz$\Rightarrow \lambda L2 = 24.4$ cm

Two services are available in the current GPS system:

SPS: The Standard Positioning Service is an open service, free of charge for worldwide users. It is a single-frequency service in the frequency band L1.

PPS: The Precise Positioning Service is restricted by cryptographic techniques to military and authorized users. GNSS satellites continuously transmit navigation signals at two or more frequencies in L band. These signals contain ranging codes and navigation data to allow users to compute both the travel time from the satellite to the receiver and the satellite coordinates at any epoch. The main signal components are described as follows:

Carrier: Radio frequency sinusoidal signal at a given frequency.

Ranging code: Sequences of zero and one which allow the receiver to determine the travel time of the radio signal from the satellite to the receiver. They are called PRN sequences or PRN codes. Navigation data: A binary-coded message providing information on the satellite ephemeris (pseudo-Keplerian elements or satellite position and velocity), clock bias parameters, almanac (with a reduced-accuracy ephemeris data set), satellite health status and other complementary information two navigation signals are provided in two different frequency bands, L1 and L2 (Enge and Misra, 1999 and Avila-Rodriguez, 2008).

2.2.2 Function of GPS

GPS operation is based on the concept of ranging and Trilateration from a group of satellites, which act as precise reference points. Each satellite broadcasts a Navigation Message that contains the following information.

The GPS system time, derived from an atomic clock installed on the satellite, with clock correction parameters for the correction of satellite time due to differences between UTC and

GPS time (the occasional ‘leap’ second added to a year) and delays (predicted by a mathematical ionospheric model) caused by the signal travelling through the ionosphere. Normally distances are calculated on GPS is based on signals of a Satellite ranging.

Distance (d) = Speed of satellite ranging (3×10^8 m/s) x time

Time (Δ t) = $t_2 - t_1$ where, t_1 = sending time, t_2 = receiving time

If travel time measures through the radio signal are the basics of GPS, then stopwatch are very working instrument in this case. In terms of Satellites, timing is perfect because the Atomic clock is the compulsory element of Satellite systems. If the three exact measurements can identify the three-dimensional position, then the fourth incorrect measure does the same thing. GPS can know the exact position of Satellites, for which can use that satellites as a reference point. So far, the calculation we are pointing to a GPS, that is sporadically. As if the whole thing was happening in a vacuum. But in reality, there are a lot of things which can be disrupt the GPS signals. To get the accurate results, this error likely to be corrected. For example, the ionosphere and atmosphere may be a reason for delay the whole function. Some error can be factored out by using arithmetic calculation and model (Ershad Ali, 2020).

2.2.3 GPS Navigation Message and segment

The Global Positioning System consists of three major segments: the Space Segment, the Control Segment, and the User Segment. The space and control segments are operated by the United States Military and administered by the U.S. Space Command of the U.S. Air Force. Basically, the control segment maintains the integrity of both the satellites and the data that they transmit. The space segment is composed of the constellation of satellites as a whole that are currently in orbit, including operational, backup and inoperable units. The user segment is simply all of the end users who have purchased any one of a variety of commercially available receivers.

2.3 The Effects of the Ionosphere on the GPS Signals

The free electrons in the ionosphere affect the propagation of radio waves. At frequencies below about 30MHz, the ionosphere acts almost like a mirror, changing the path traveled by radio wave back towards the Earth, thereby allowing long-distance communication. However at higher frequencies, such as those used by the GPS, radio waves could pass through the ionosphere but are affected (slow down) by it. The ionosphere is more difficult to model because of its unusual shape and the number of factors that affect it. A model has been developed that requires eight variable coefficients. Every day, the control segment calculates the coefficients for the ionospheric model and uplinks them to the satellites. Severe

scintillation of the GPS satellite signals can result in loss of satellite tracking, which degrades GPS positioning accuracy. Even when satellite tracking is maintained, scintillation can cause errors decoding the GPS data messages, cycle slips, and ranging errors. GPS signals that transmit from the satellite at a distance of 20,183 km, passes through a vacuum until they reach the last few percent of their journey. The signals encounter the bulk of free electrons around 350 km, and it is these particles that affect the speed at which the signal propagates (Abidin, 2008). The signals travel at a velocity of light through space, but they are slowed slightly by varying degrees in direction as they pass through the ionosphere (G. S. Kumar *et al*, 1998 and B. R. Elbert, 2004]. Regular and unusual solar activity can produce variations in the effect of the ionosphere on GPS signals results in errors at atmospheric height of about 100 km. The receiving signals will cause the receiver to have ranging errors such as ephemeris data, satellite clock, pseudo range and multipath.

The TEC is the amount free electrons along the path of the electromagnetic wave between each satellite and the receiver, given by;-

$$TEC=\int_{reciever}^{sattelite} N(s)ds \qquad (2.\ 2)$$

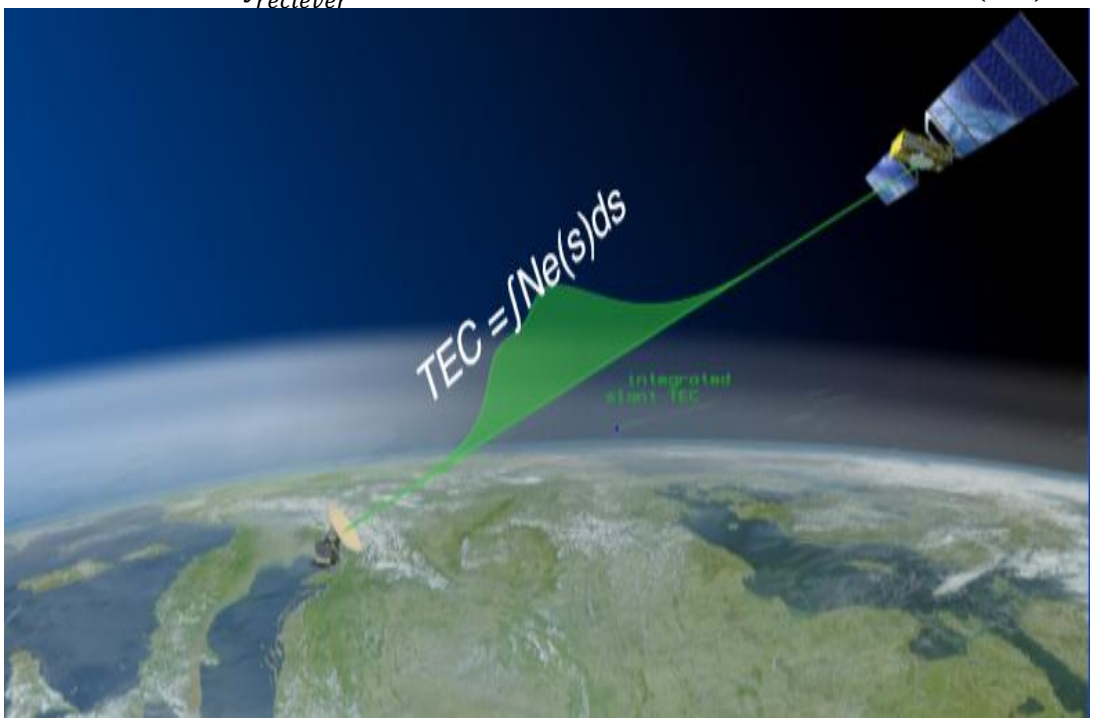

Figure 2. 2: *Path of total electron content from satellite to receiver (J. Louis J. Ippolito, 2008)*

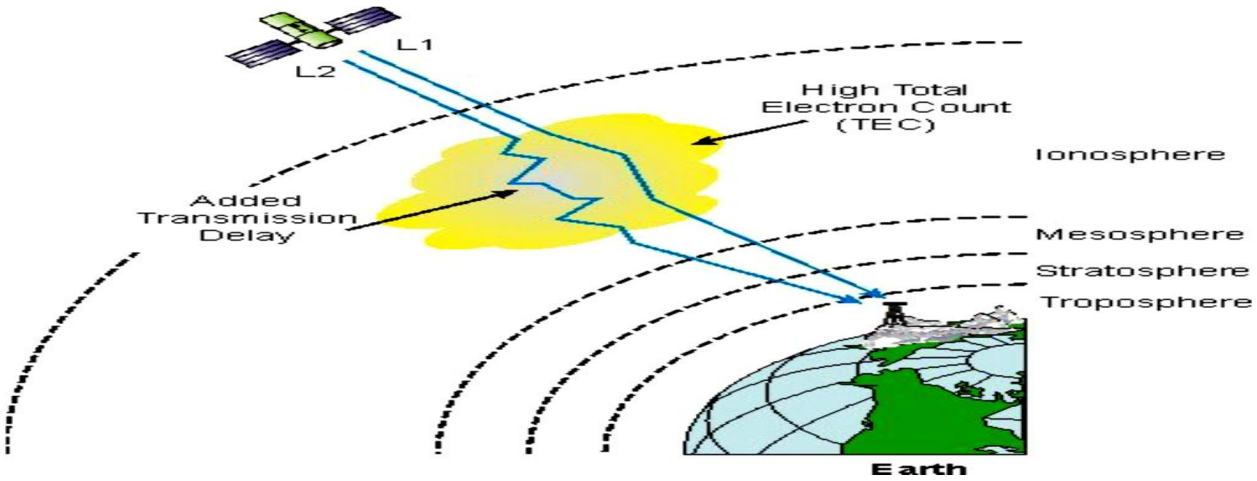

***Figure 2.3**: Signal affected at ionosphere region (Ledvina, 2004)*

Propagation that causes signals delay in the presence of ionosphere results in increased errors in position and navigation Scintillation effects caused losses of signal due to small-scale irregularities in the ionosphere.

The ionospheric errors equations GPS approach can be written as

$$\mu=1-\alpha\frac{N}{f2} \qquad (2.3)$$

Where, $\alpha= 40.3 m^2/s^2$

N is the free electrons density per cubic meter•

μ is the ionospheric group delay with respect to propagation in vacuum

f is the radio wave frequency in GHz.

Note that, effect of ionospheric refraction index is inversely proportional to the square frequency that causes a delay in time Δt that is:

$$\Delta t_i=\frac{1}{C}\int_T^R(\mu-1)dl=\frac{\alpha}{Cf2}\int_T^R N(s)ds \;=\; \frac{40.3}{Cf2}\,\mathrm{TEC} \qquad (2.4)$$

The quantity $N(s)ds$ is the Total Electron Content (TEC), in electrons per square meter, integrated along the signal path between transmitter (T) and receiver(R), C is the speed of light (Kintner and Ledvina, 2004, Klobuchar, 1988). In carrier phase measurements, the effect causes a phase advance leading to an underestimated (shorter) range.

The largest effect that ionosphere has on GPS accuracy is group time delay which is proportional to the total electron content (TEC). The ionosphere predominantly affects GPS radio communication. This is largely due to the presence of random electron density fluctuations within the ionosphere. The ionosphere contains irregularities of many sizes. When GPS signal propagates through these irregularities it experiences amplitude and phase scintillations, which degrade the strength of the received signal.

The speed of propagation of radio wave at some point in the ionosphere is determined by the electron density present. The phase of the carrier speed is actually increased by the presence of the electrons. The greater the density of the electrons, the greater is the speed of the carrier phase. The overall effect on a radio wave is obtained by integrating the electron density along the whole path that a signal follows from a satellite to a receiver. The result is that a particular phase of the carrier arrives at the receiver earlier than it would have had the signal traveled from the satellite in a complete vacuum. This early arriver is known as phase advance. On the other hand, the modulating signal of the carrier (the pseudorandom noise codes and navigation message) is delayed by the ionosphere which increases the apparent length of the path travelled by the signal. The delay of the modulation is called the group delay. The size (error) of the phase advance and the group delay are equal in magnitude and opposite in signs. Both are proportional to the TEC and inversely proportional to square of the carrier frequency. The higher the frequency the smaller is the effect (Klobuchar, 1996).

The appearance and disappearance of dark, irregularly shaped areas known as sunspots are characterized by strong magnetic fields. These sunspots cause variations in the ionization level of the ionosphere. Sunspots tend to appear in two cycles, every 27 days and every 11 years.

2.4 Ionization profile of earth's upper atmosphere

The researcher will derive the ionization production function of the atmosphere in the following. Assume the solar radiation penetrates the target horizontally stratified medium, and that medium obeys the equation of state for an ideal gas law. For a neutral atmospheric gas in hydrostatic equilibrium, the particle density (m^{-3}) will decrease by an altitude with constant scale height in a given atmosphere:

$$n = n_o \exp\left(-\frac{z}{H}\right) \qquad (2.5)$$

The incoming solar radiation has a wavelength λ and it creates intensity λ at an altitude of z. The unit of intensity is $m^{-2}s^{-1}$ and has a cross-sectional area σ measured in (m^2) for ionizing neutral particles in the atmosphere by radiation at wavelength 'λ' Ionize several neutral particles per cubic meter and second by a solar radiation of wavelength 'λ' . Assume the radiation with intensity I (λ, Z) has passed a distance through the atmosphere; the intensity will be decreased if it passes through an extra infinitesimal distance (Figure 2.10) through a slab of the atmosphere. This reduction has to be proportional to the intensity of the solar radiation, the cross-section for the ionization, and the number of targets that can be ionized.

The decrease of 'I' per unit distance is as follows: Let the intensity of the solar photon radiation at wavelength λ be I (λ, z) in units of photons m^{-2} s^{-1} at an altitude z.

$$I=\frac{N_{ph}}{At} \qquad (2.\ 6)$$

Where N_{ph} is the number of photons incident to be A, t is the time. The number of neutral molecules in the slab is

$$N_T=nAds \qquad (2.\ 7)$$

Where n is the number density of the neutral molecules. If the absorption cross-section of a single molecule in units of m^2 is σ, the total absorption cross-section of the slab is

$$\sigma_T=N_T\sigma=\sigma nAds \qquad (2.\ 8)$$

The number of photons incident to the slab per unit time is

$$\frac{N_{ph}}{t}=IA \qquad (2.\ 9)$$

The number of absorbed photons per unit of time is determined by the ratio

$$\frac{\sigma_T}{A}=\sigma nds \qquad (2.\ 10)$$

$$Nabph=(\frac{Nph}{t})(\frac{\sigma T}{A})=(IA)(\sigma nds)=IA\sigma\ nds \qquad (2.\ 11)$$

The absorbed intensity (absorbed photons per unit area per unit time) is

$$Iab=\frac{Nabph}{A}=I\sigma\ nds \qquad (2.\ 12)$$

The intensity 'I' left after propagating through the slab is given

$$I'=I-Iab=I-I\sigma\ nds \qquad (2.\ 13)$$

The decrease in intensity (the change in intensity) is given by

$$dI=I'-I=(I-Iab)-I=(I-I\sigma\ nds)-I=-I\sigma\ nds \qquad (2.\ 14)$$

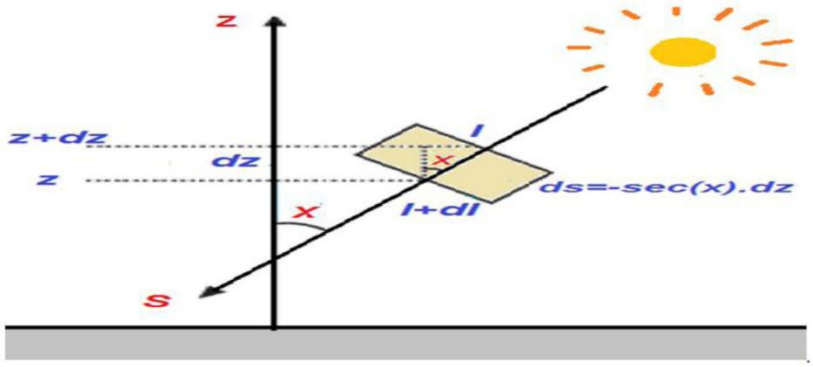

Figure 2. 4: *Schematic diagram of an illustration of the geometry related to the solar irradiation (I) when penetrating a slab of thickness dz in the Earth's atmosphere at a Zenith angle (Brekke, 2013)*

From eq. (2.10) the rate of decrease of intensity per unit distance is given by

$$\frac{dI}{ds} = - n\sigma I \qquad (2.\ 15)$$

If the intensity enters the atmosphere at a zenith angle ϰ, for every unit of energy absorbed by radiation, there will be formed several C electrons. Then the production of electrons per cubic meter and second can be expressed as follows:

$$q=CnI\sigma=-C\frac{dI}{ds} \qquad (2.\ 16)$$

C is called the ionization efficiency. For atomic species, the ionization efficiency C is unity, so all the energy of the radiation goes into producing ion-electron pairs; for molecules, however, < 1. We analyze that n increases and I decrease then the product of n. I maximum somewhere (figure 2. 11), and this maximum is found:

$$\frac{dq}{ds}=-C\sigma\left(I\frac{dn}{ds}+n\frac{dI}{ds}\right)=0 \qquad (2.\ 17)$$

Since C and σ are constants and introducing the index m for the maximum we can get:

$$\frac{1}{n_m}\left(\frac{dn}{ds}\right)_m + \frac{1}{I_m}\left(\frac{dI}{ds}\right)_m=0 \qquad (2.\ 18)$$

If radiation falls towards the atmosphere with respect to the zenith angle X (Figure 2.10), the researcher sees that

$$ds=-\frac{dz}{\cos X} \qquad (2.\ 19)$$

$$\frac{1dn}{nds}-\frac{1dn}{ndz}\cos X \qquad (2.\ 20)$$

And by substituting n from (2.1) into (2.16) the researcher can get:

At any distance s and the maximum production:

$$\frac{1}{n_m}\left(\frac{dn}{ds}\right)_m=\frac{\cos X}{H} \qquad (2.\ 21)$$

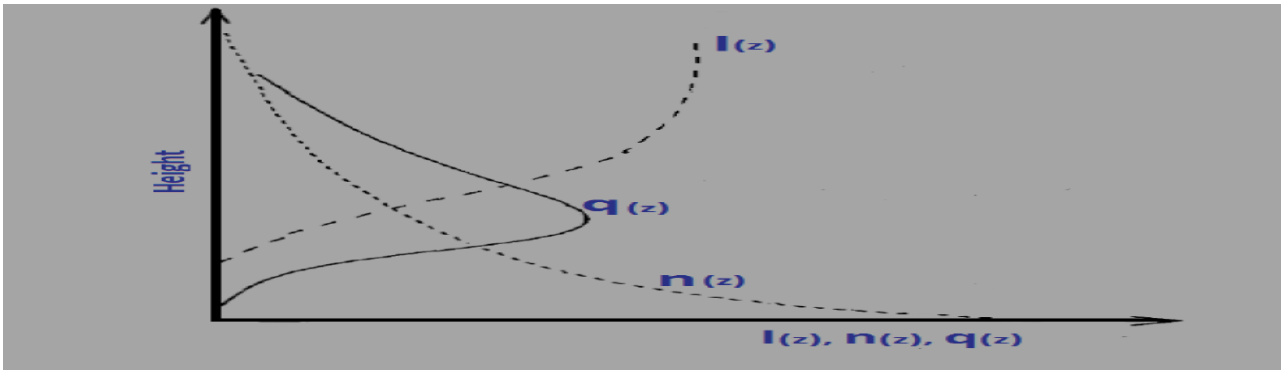

Figure 2. 5*: *Solar irradiation of intensity I decrease due to absorption downward in the Earth's atmosphere where the density increases towards the Earth.

A maximum ionization rate q therefore occurs at the altitude of cross-over points of the two curves I(z) n(z)and) are situated (Brekke, 1997)

From equation (2.11) we find at this maximum

$$\frac{1}{n_m}\left(\frac{dn}{ds}\right)_m = -n_m\sigma \qquad (2.\ 22)$$

Substituting (2.18) and (2.19) into (2.14) the researcher can get the following result;

$$\frac{\cos X}{H} = n_m\sigma \qquad (2.\ 23)$$

And then lastly

$$H.n_m.\sigma\ \sec X = 1 \qquad (2.\ 24)$$

We know from previously equation (2.1)) that for an atmosphere with a constant scale height.

$$H.n_o = N \qquad (2.\ 25)$$

Where N is the total number per unit area between the reference height and infinity and also focuses at maximum ionization, therefore

$$H.n_o = N_m \qquad (2.\ 26)$$

Nm is the number of neutral particles above a unit area at height Z_m in the atmosphere and equation (2.21) becomes

$$N_m.\sigma.\sec X = 1 \qquad (2.\ 27)$$

Substituting (2.15) into (2.1) we find:

$$\frac{1dI}{Ids} = -\frac{1dI}{Idz}\cos X = -\sigma n = -\sigma.n_o \exp\left(-\frac{z}{H}\right) \qquad (2.\ 28)$$

And

$$\frac{dI}{I} = +\sigma.n_o.\exp\left(\left(-\frac{z}{H}\right).\sec X.dz\right) \qquad (2.\ 29)$$

At the source of radiation

$$Z = Z_\infty,\ I = I_\infty$$

$$\int_{I\infty}^{I}\frac{dI}{I} = \sigma n_o.\sec X\int_{\infty}^{z}\exp\left(-\frac{z}{h}\right)dz \qquad (2.\ 30)$$

And

$$ln\frac{I}{I\infty} = -\sigma.n.H.\sec X \qquad (2.\ 31)$$

At the maximum height of ionization, therefore

$$\ln\frac{I_m}{I\infty} = -\sigma.n_m.H.\sec X = -1 \qquad (2.\ 32)$$

$$I_m = \frac{I_\infty}{e} \qquad (2.\ 33)$$

The radiation intensity decreased by 1/e at the height of the maximum ion production.

Generally,

$$I=I_{\infty}\exp(-\sigma nH\sec X)=I_{\infty}\exp(-\tau) \quad (2.\ 34)$$

The optical depth is given by

$$\tau = \sigma n.H.\sec(X) \quad (2.\ 35)$$

At the height of maximum ionization the optical depth is;

$$\tau_m=\sigma n_m.H.\sec(X) = \sigma n_o \exp\left(\frac{-z_m}{H}\right) H.\sec(X) = 1 \quad (2.\ 36)$$

And

$$\exp\left(\frac{z_m}{H}\right) =\sigma.n_o H.\sec X \quad (2.\ 37)$$

The sun is overhead (X= 0)

$$\exp\left(\frac{z_{m,o}}{H}\right) =\sigma.n_m.H.\sec X \quad (2.\ 38)$$

Therefore

$$\exp\left(\frac{z_m}{H}\right) = \exp\left(\frac{z_{m,o}}{H}\right) \quad (2.\ 39)$$

And

$$\frac{z_m}{H} = \frac{z_{m,o}}{H} + \ln \sec X \quad (2.\ 40)$$

The maximum ion production height increases as the zenith angle increases and the lowest height $Z_{m,o}$ and the sun reaches overhead. Combine (2.21), (2.28), (2.29) the researcher find;

$$\ln\frac{I}{I_m} - (n-n_m)\,\sigma.n_o H.\sec X = 1-\frac{n}{n_m} \quad (2.\ 41)$$

And finally

$$\frac{I}{I_m}= \exp\left[1-\frac{n}{n_m}\right] \quad (2.\ 42)$$

This indicates the relationship between the intensity of the radiation at a given neutral density relative to the intensity and neutral density at the maximum of ionization.

2.5 Ionization rate

The maximum ion production rate is according to equations (2.12), (2.21), and (2.29) given:

$$q_m=C.\ n_m.\ \sigma_m = C.\ .\ \sigma_m = \frac{I_{\infty}}{e} = C.I/e.H\cos\square \quad (2.\ 43)$$

When the sun is overhead (X= 0) we can find

$$q_{m,o} = \frac{C.I}{e.H} \quad (2.\ 44)$$

And therefore

$$q_m = q_{m,o} \cos X \qquad (2.45)$$

At maximum production can never be larger than for the Sun is overhead, and it decreases as cos□ for zenith angle 'X' increase. The rates of ion production we can take the following ratio by using (2.12) and (2.39) and introducing (2.40):

$$\frac{q}{q_m} = \frac{C.n.\delta.I}{C.n_m.\delta.I_m} = \frac{n}{n_m} \exp^{(1-n/nm)} \qquad (2.46)$$

We can also perform another ratio by using (2.1) as a reference

$$\frac{n}{n_m} = \exp\left(\frac{-z-z_m}{H}\right) \qquad (2.47)$$

We can express the production q at height z in the following way;

$$q=q_m \exp\left(\frac{-z-z_m}{H}\right) H) \exp\left[1- \exp\left(\frac{-z-z_m}{H}\right)\right] \qquad (2.48)$$

Or

$$q=q_m \exp\left[1-\frac{z- z_m}{H}-\exp\left(\frac{-z- z_m}{H}\right)\right] \qquad (2.49)$$

Inserting the normalized reduced height into the maximum ionization height

$$y =\frac{z-z_m}{H} \qquad (2.50)$$

$$q=q_m \exp [1-y-\exp (-y)] \qquad (2.51)$$

Substituting Zm/H from (2.36) into (2.45) we get the following

$$q = q_m \exp\left[1-\frac{z-z_{m,o}}{H} + \ln \sec X -\exp\left(\frac{z-z_{m,o}}{H} +\ln \sec X\right)\right] \qquad (2.52)$$

$$q = q_m \sec X.\exp\left[1 - \frac{z-z_{m,o}}{H} - \sec X.\exp\left(\left(\frac{z-z_{m,o}}{H}\right)\right)\right] \qquad (2.53)$$

And then applying (2.41) it gives:

$$q =q_{m,o} \exp\left[1-\frac{z-z_m}{H} -\sec X.\exp\left(-\frac{z-z_m}{H}\right)\right] \qquad (2.54)$$

By representing the normalized height $X = \frac{z-z_{m,o}}{H}$ reduced to maximum ionization height when the sun is overhead we find

$$q = q_{m,o}\exp (1-X - secX\exp(-X)) \qquad (2.55)$$

The value of □ is large and (Z>>Zm,o) the form of the profile is:

$$q\approx= q_{m,o}\exp\left(-\frac{z}{H}\right) \qquad (2.56)$$

Zenith angle X (Figure 2.10), we see that the profile itself decays by altitude (height) as the density of the target atmosphere above the maximum value of the ionization profile. The value of X > 2 (i.e., at a distance more than two scale heights above Zm,o). This relation arises due to the aiming height intensity of the radiation is only weakly decreased, and the rate of production is essentially proportional to the density of the target gas. The value of □ is very large negatively and (z <<Zm,o) the form of production rate and the profile

decreases very quickly with height below the altitude of the peak and looks like mathematically in the following way (Brekke A. , 2013).

$$q = q_{m,o} \exp[-\sec X . \exp(-\frac{z - z_{m,o}}{H})] \quad (2.57)$$

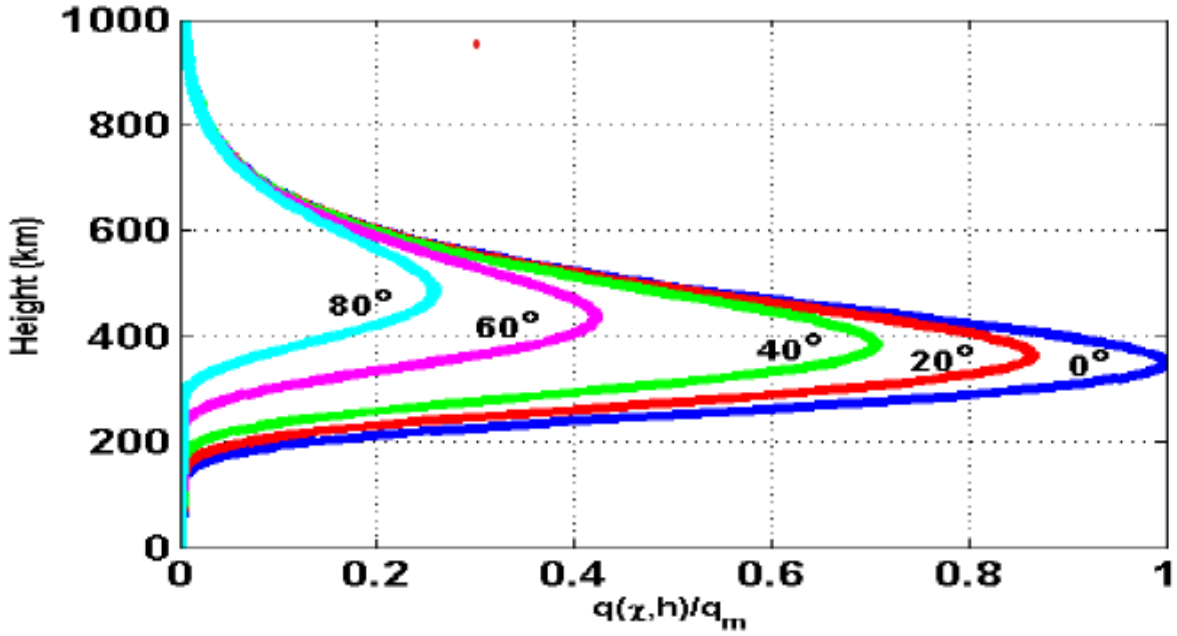

Figure 2. 6: *Chapman ionization profile for different zenith angles and maximum ionization production occurred when the sun is over head.*

CHAPTER THREE

IONOSPHERIC MODEL AND gLAB SOFTWARE

3.1 gLAB software

Nowadays, GNSS systems are a crucial component of the global information infrastructure enabling broad new market capabilities and facilitating innovation in efficiency, safety, environmental, science and public security.

The requested Educational GNSS Software Tool constitutes a step forward in the ESA-Education Office aim at fostering the transfer of knowledge in GNSS through the provision of GNSS-based educational utilities. The good consecution of this objective will help to enhance the GNSS knowledge of European students and professionals. The research group of Astronomy and Geomatics (gAGE) from the Universitat Politecnica de Catalunya (UPC) has developed the GNSS-Lab (gLAB) tool suite, which is an interactive educational multipurpose package to process and analyses GNSS data. This software package is targeting the following groups of users for education professionals aiming to teach GNSS from both a theoretical and practical points of view, Standalone students and professionals with basic knowledge on GNSS as a self-learning tool, and Professionals with more in deep knowledge on GNSS who want an easy and user-friendly tool with precise positioning capability (Hernandez-Pajares *et al*., 2014).

3.1.1 General software characteristics

This tool performs a precise modelling of the GNSS observables (pseudo range and carrier phase) at the centimeter level, allowing both standalone GPS positioning (SPP) and PPP. The first release of this software package implements full processing capabilities for GPS data and is prepared to incorporate future module updates, such as an expansion to Galileo and GLONASS systems, EGNOS and differential processing. The gLAB software is capable of reading a variety of standard formats like Station measurements from Observation RINEX standard version 2.11 and 3.00, Broadcast message from Navigation RINEX standard version 2.11 and 3.00, Satellite clocks from Clocks RINEX standard, Satellite orbits and clocks from SP3 standard, Ionospheric maps from IONEX standard. o Constellation status (with information between Satellite Vehicle Number (SVN) and PRN) of the satellite, Antenna Phase Center information from ANTEX standard, Differential Code Biases from precise .DCB files and, Receiver type information from GPS Receiver (Sanz *et al*., 2020). File Types Moreover, functionality is also included for GPS, Galileo and GLONASS, allowing performing some data analysis with real multi-constellation data. The tool is able to run

under Linux and Windows operating systems (OS). It is programmed in C and Python languages and is divided in three main software modules. The gLAB tool features a wide range of characteristics only available in advanced GNSS data processing software.

3.2 How gLAB mode work?

Work modes gLAB can work in four different modes:

Positioning Mode: 'Standard' mode, where all the processing is done and the position solution for a receiver is provided as OUTPUT messages. The minimum parameters required for this mode are an input observation file (input: obs) and orbit and clock products (input: nav, input: SP3 or input: orb/'input: clk'). Using precise products will also require the use of an ANTEX file (input: ant').

Show Input Mode: This mode only reads an input RINEX observation file and prints its measurements. The parameter required for this mode is input: obs, and specifically, no orbit nor clock products should be provided (if provided, gLAB will switch to Positioning Mode).

Product Comparison Mode: This mode reads and compares two different sources of orbit and clock products. In order to use this mode, input: obs' must be avoided, and two different orbit and clock products should be provided.

Show Product Mode: This mode reads a single source of orbit and clock products. In order to use this mode, input: obs' must be avoided, and a single orbit and clock product should be provided. This mode output SAT messages.

The initial screen can be seen in Fig. 3.1, where two main tabs may be found:

Positioning: Interfaces with the DPC tool, and allows selecting the different processing options.

Analysis: Interfaces with the DAT tool, and allows selecting the plotting options.

Figure 3.1: *gLAB GUI initial screen (Hernandez-Pajares, 2021)*

The DPC implements all the data processing algorithms and can be executed in command line. The DAT provides a plotting tool for the data analysis. The GUI consists in different graphic panels for a user friendly managing of both the DPC and DAT. Both the DPC and DAT modules may be used independently of the GUI, including them in batch files to automatically process GNSS data (Hernandez-Pajares *et al*., 2014). .

The GUI also provides two data processing templates, shown as buttons in the lower center part of the interface with labels SPP Template and PPP Template see Fig. 3.2. Those templates" automatically configure the appropriate options to carry out the desired data processing strategy. SPP template GNSS single point positioning that depend on single frequency receiver. GNSS positioning uses technique of one-way ranging and it is based on measures of distance between satellites (known position) and receiver (unknown position), given by:

$$\rho = \sqrt{(X_r - X_s)^2 + (y_r - y_s)^2 + (z_r - z_s)^2} \qquad (3.\ 1)$$

ρ is pseudorange (measured)

X_s , y_s , z_s are satellite coordinate (known)

X_r , y_r, z_r are receiver coordinate unknown

If the number of measurements available is equal to the number of unknowns, the solution is uniquely determined; if the measurement number is greater than unknown number, the solution could be calculated according to the optimization criterion.

To achieve a good positioning, raw pseudorange measurement must be corrected for the satellite clock error, relativity effects, and atmospheric delays, according to the equation:

$$\rho_c = \rho + cdt_s + cdt_r - cdT_R - d_{Iono} - d_{tropo} \quad (3.2)$$

Where d_{Iono} is is the ionospheric delay,

d_{tropo} is the tropospheric delay

cdt_r is the relativistic effect correction term,

cdt_s is the satellite clock bias including TGD (Time Group Delay),

ρ is uncorrected pseudorange measurement

ρ_c is the corrected pseudorange measurement,

3.2.1 Positioning tab

The positioning tab is split into 5 different sections, which correspond to five different modules inside the DPC:

Input: It is like a driver" between the input data and the rest of the program. This module implements all the input reading capabilities and stores data into the appropriate internal structures.

RINEX Observation File: Source GNSS measurements data file in RINEX format (version 2.11 or 3.00) and ANTEX File: Antenna phase center information for both GNSS satellites and receiver antennas

Figure 3.2: *gLAB GUI initial Positioning tab (Segura, 2014).*

Preprocess: This section provides all the configuration options to preprocess the input data. In particular, it allows changing the decimation rate, the elevation mask, the cycle-slip detection, and selecting individual satellites for the processing. Data Decimation [s]: This option will decimate the input data at the specified rate. Data gap[s] is parameter sets the maximum period of time (in seconds) allowed between two consecutive data samples. Therefore, a larger period of time between data samples will automatically declare a cycle-slip.

Model: The following options allow to enable/disable the different models included in the processing.

The satellite clock errors correspond to the clock synchronism errors of the satellite clocks in relation to the GNSS system time scale. These errors depend heavily on the type of oscillator of the satellite and are quite unpredictable. They can only be obtained by some kind of estimation. This module has all the functions to fully model the receiver measurements. It implements several kinds of models, which can be enabled or disabled at will.

Broadcast (same as navigation): For Klobuchar ionospheric model, use the same broadcasted file as for the orbits and clocks for the Klobuchar parameters. Broadcast (specify), for Klobuchar ionospheric model, specify a different broadcasted file to use for the Klobuchar parameters. This option is also useful when using SP3 and correcting ionosphere. A priori

receiver position is initial receiver position. This is used to linearize the filter and to obtain the values for the models.

Figure 3.3: *gLAB modeling tab (Klobuchar, 1988).*

Filter: This module implements a configurable Kalman filter, and obtains the estimations of the required parameters.

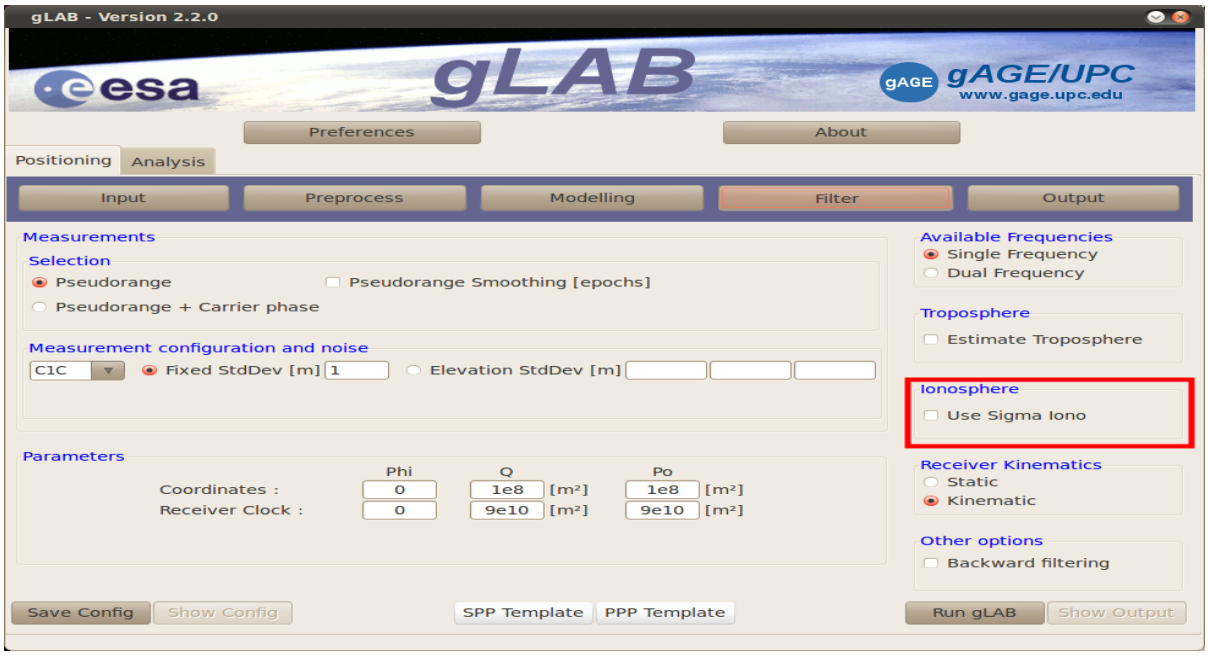

Figure 3.4: *gLAB filter tab (Klobuchar, 1988).*

Out put

The OUTPUT message type gives the position obtained by the filter differenced with this apriori position. So if this position is accurate enough, the difference can be used as a direct measure of the error. Specify the receiver position in XYZ components (in meters) or geodetic components (in degrees and meters). Provide a reference position file, the position of this file will be used as a priori position and for computing the differential fields in the OUTPUT message. If used calculate do not provide a priori position, gLAB will calculate it. Use RINEX Position: Use the APROX POSITION XYZ field of the RINEX of measurements (Sanz *et al*., 2020).

Auxiliary files: User can provide different auxiliary files: to get information about the receiver and to correct the Differential Code Biases (DCB) which are the delays due to electronic, antennas and cables of receiver and transmitter devices which directly affect the measurements with a bias.

P1 – P2 DCB Source files: Broadcast (same as navigation): Use the same RINEX navigation file for the DCB computations than the orbit and clock product source. Broadcast (specify): Specify a different RINEX broadcasted file to obtain the codes (P1 – P2) digital bias. Precise .DCB file: Specify DCB file for the (P1 – P2) biases for all satellites.

P1 – C1 DCB Source files: Receiver Type file: Specify a file with the receiver type information: Receivers, Antennas, Radomes, and Antenna+ Radome manufacturer's name, model and code. Precise .DCB files Specify a .DCB file for the (P1 – C1) biases for all satellites. User added error files, columnar text file which indicates the user defined error that gLAB must add to measurements.

RUN button, execute the DPC program with all the configured parameters of the Calculus tab. This button can be used in all Input, Preprocess, Modeling, Filter and Output sections

.This module outputs the data obtained from the FILTER. That give. Show Output button: Opens a text editor of the output of the last execution of gLAB

I. KML (Keyhole Markup Language)

KML is an XML-based format used for representing geographic data in applications such as Google Earth and other mapping software.

Usage in gLAB:

KML files generated by gLAB allow users to visualize GNSS position solutions and trajectories on maps. A KML file typically includes point data (positions), paths, and possibly additional information such as timestamps and accuracy metrics. Users can interact

with the KML files, enabling functionalities like zooming in/out and exploring data points in a geographic context.

II. SP3 (Standard Product 3)

SP3 is a file format used primarily for storing precise satellite ephemeris data, which describes the orbits of GNSS satellites. It use in gLAB for; Ephemeris Data**,** SP3 files contain information about satellite positions and velocities at specific times, which is crucial for accurate GNSS positioning. Time Reference**:** The data is time-stamped and can include both GPS and GLONASS satellite information. Integration**:** SP3 files can be used alongside GNSS measurements for post-processing, enabling improved accuracy by providing precise satellite orbit information.

For overall both KML and SP3 files play essential roles in GNSS data processing with gLAB. KML files facilitate visualization of positioning data, while SP3 files provide critical satellite ephemeris information necessary for accurate positioning and navigation (Klobuchar, 1988).

3.2.2 Analysis tab

The analysis tab allows configuring all the visualization options for the DAT, as shown in Fig. 3.5. There are two different areas. On the upper part, the user finds all the templates buttons. In this case, the templates are a set of preconfigured plotting options for the Graphic Details section. Clicking on any button will load all the corresponding options, allowing modifying or plotting them directly.

On the lower part, the user can configure a plot from scratch using the Global Graphic Parameters section below the templates. The GUI can accommodate up to four plots, (i.e. four different data series in the same graphic) although the DAT program has no plot number limitation when executed independently from the command line.

Finally, it is only to be remarked that while there are some common data that needs to be uploaded only once per graphic, user can fine tune different options of the individual plots, providing full flexibility (Segura, 2014).

Figure 3.5: *gLAB GUI initial Analysis tab. (Segura, 2014)*

The available templates are:

NEU position error: The NEU position error template sets the options to print the three components (North, East and Up) of the error of the receiver positioning obtained by the filter. This error is computed by the difference between the direct filter estimation and the apriori receiver position in the input section. Hence, in order to obtain reliable error estimation this apriori position should be precise. North-East dispersion: The North-East dispersion template sets the options to print the North vs. East position error components. This provides an insight of the horizontal dispersion and biases of the errors.

3.3 Ionosphere model

Focusing now on the ionosphere, it is the atmosphere region extends from a height from 50 to 2000 km above the Earth. This region contains a partially ionized medium, as a result of solar X and Extreme Ultraviolet (EUV) rays in the solar radiation and the incidence of charged particles, which ionize the different neutral atmospheric components.

The propagation speed of GNSS electromagnetic signals in the ionosphere de- pends on its electron density, which is typically driven by two main processes. During the day, the Sun's radiation ionizes neutral atoms to produce free electrons and ions. During the night, the recombination process prevails, where free electrons are recombined with ions to produce

neutral particles, which leads to a reduction in the electron density. The electron density (N_e) in the ionosphere changes with height, having a maximum of;

$N_e \approx 10^{11}$ to 10^{12} $\frac{e^-}{m^3}$ around 300-500km.

The ionosphere is a dispersive medium, which means that it is frequency dependent. Furthermore, dispersive mediums reflect signals lower than a threshold frequency. For the ionosphere the threshold is at 10^6 Hz, which is lower than GNSS signals, that are at the order of 1GHz (= 10^9 Hz), thus allowing satellite signals to go through.

To compute the difference between the measured range (with frequency f signal) and the Euclidean distance between the satellite and receiver, the relation is the following (Sanz *et al*., 2013):

$$\Delta_{ph,f}^{iono} = -\frac{40.3}{f^2}\int N_e dl, \quad \Delta_{gr,f}^{iono} = +\frac{40.3}{f^2}\int N_e dl, \qquad (3.3)$$

The differences $\Delta_{ph,f}^{iono}$ and $\Delta_{gr,f}^{iono}$ are called the phase and code ionospheric refraction, respectively, and the integral is defined as the Slant TEC, or Slant Total Electron Content (STEC)

$$\text{STEC} = \int N_e dl \qquad (3.4)$$

Where, phase measurements are advanced on crossing the ionosphere, that is a negative delay, while the code measurements undergo a positive delay.

Usually, the STEC is given in TEC unitfs (TECUs), where 1TECU = 10^{16} e − /m 2 and the ionospheric delay I_f (at the frequency f) is written as;

$$I_f = \alpha_f \text{ STEC (in meter)}, \qquad (3.5)$$

Where, $\alpha_f = \frac{40.3}{f^2}(10^{16})$ (f is in Hz)

Single frequency receivers need to apply a model to remove ionospheric effects. Ionosphere effects are greatly variable; hence it is necessary to adjust model parameters periodically. GPS and, BeiDou broadcast these parameters through the navigation file transmitted by the satellites, and are updated daily (Vinh *et al*., 2013)GLONASS does not broadcast any ionospheric model, but any of the existing models can be applied to this constellation by applying a correction factor given by their relative squared frequency ratio.

3.3.1 Klobuchar model

The Klobuchar model (Klobuchar, 1988) is a simple broadcast ionospheric model built on a simple cosine representation of the ionospheric delay. The model was designed based on Bent model (Llewellyn and Bent, 1973). Due to the simplicity of model structure, it has been widely used in many single frequency GNSS positioning and navigation applications. The

period and amplitude of the ionospheric delay are represented as third degree polynomials in local time and geomagnetic latitude. The eight time-varying coefficients of the model are broadcast in the GPS navigation message (Farah, 2008).

The Klobuchar model is generally formulated with monthly median parameters and can only predict the long-time average conditions of the ionosphere (Wang *et al*., 2016 and Dodson, 1988) concluded that the correction accuracy of the model is about 50-60% of the total delay. The model is unable to show any significant fluctuations from day to day as it assumes an ideal smooth behavior of the ionosphere (Farah, 2008). (Newby *et al*., 1990) concluded also that the range error by the model can be of order of 50 m under severe ionosphere activity at low elevations. This model is independent from user's position (it does not apply any specific correction for any region) and the ionosphere is modeled as single layer at an altitude of 350 km. This model assumes there is a constant delay of 5 ns during night time and a half-cosine function in daytime that is centered at the 14th hour (2 pm) of local time as shown in Fig. 3.6, whose amplitude and period are given as a function of the eight parameters broadcasted in the navigation message.

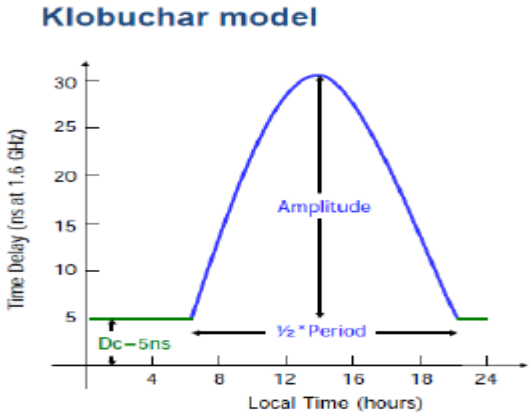

Figure 3.6: *Klobuchar model layouts (Sanz, 2013)*

Klobuchar and BeiDou satellites broadcast the parameters of the Klobuchar ionospheric model for single-frequency users. The Klobuchar model was designed to minimize user computational complexity and user computer storage so as to keep a minimum number of coefficients to be transmitted on the satellite–user link. This broadcast model, initially developed for GPS, is based on an empirical approach [Klobuchar, 1987] and is estimated to reduce the RMS ionospheric range error by about 50% worldwide. It is assumed that the electron content is concentrated in a thin layer at 350km in height (375km is taken in Beidou). Thus, the slant delay is computed from the vertical delay at the Ionospheric Pierce Point (IPP) by multiplying by an obliquity factor (i.e. the mapping function),

3.3.1.1 Klobuchar Algorithm Equations

The Klobuchar algorithm to run in a single-frequency receiver is provided as follows [Klobuchar, 1987].

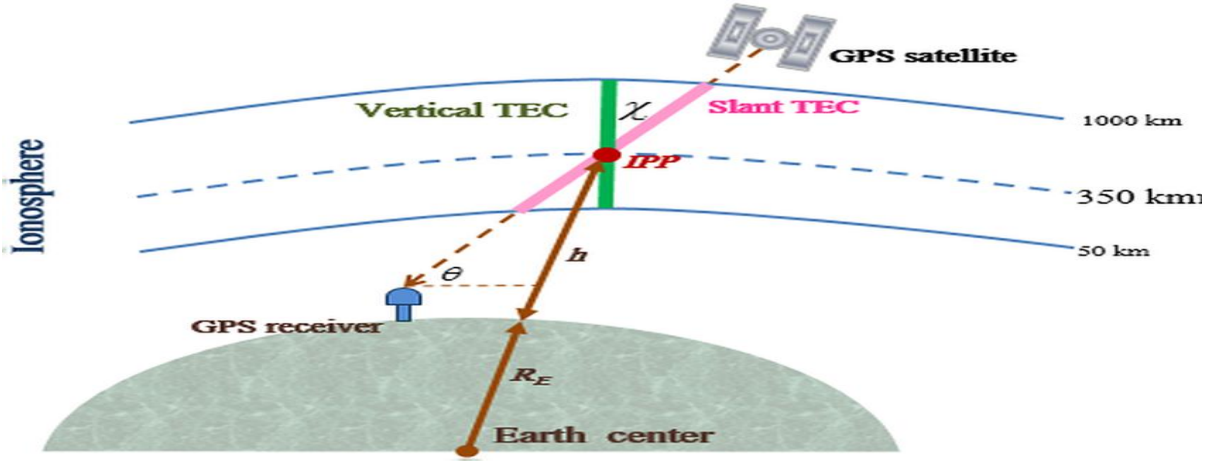

Figure 3.7: *Ionospheric Pierce Point (IPP), vertical and slant delay illustration (Yilma, 2024)*

Given the user's approximate geodetic latitude φ_u and longitude λ_u, the elevation angle E and azimuth A of the observed satellite and the Klobuchar coefficients α_n and β_n broadcast in the GPS or Beidou satellite navigation message

1. Calculate the Earth-center angle

$$\psi = \frac{\pi}{2} - E - \arcsin\left(\frac{R_E}{R_E+h}\cos(E\right) \quad (3.6)$$

Computing latitude of the IPP

$$\phi_1 = \arcsin(\sin\varphi_u \cos\psi + \cos\varphi_u \sin\psi \cos A) \quad (3.7)$$

Computing longitude of the IPP

$$\Lambda_I = \lambda_u + \frac{\sin\psi \sin A}{\cos\phi 1} \quad (3.8)$$

Find geomagnetic latitude

$$\Phi_m = \arcsin(\sin\phi_1 \sin\phi_p + \cos\phi_1 \cos\phi_p \cos(\lambda_I - \lambda_p)) \quad (3.9)$$

With $\phi_p = 78.3°$, $\lambda_p = 291°$ the coordinate of geomagnetic pole

Find local time at IPP

$$t = 43200 + \frac{\lambda I}{\pi} + t_{GPS} \quad (3.10)$$

(λ_I in radian, t in second)

Where $0 \leq t \leq 86400$

If $t \geq 86400$, subtract 86400. If $t < 0$, add 86400.

Compute the amplitude of ionospheric delay

$$A_I = \sum_{n=0}^{3} \alpha_n \left(\frac{\Phi m}{\pi}\right)^n \text{ (in second)} \quad (3.11)$$

If $A_I < 0$, then $A_I = 0$

The height of the ionospheric layer is taken as 350km for GPS and 375km for BeiDou. R_E =6378km.That is, the latitude of the projection on Earth of the IPP with the ionospheric layer.

Compute the period of ionospheric delay

$$P_I = \sum_{n=0}^{3} \beta_n \left(\frac{\Phi m}{\pi}\right)^n \text{ (in second)} \quad (3.12)$$

If $P_I < 72000$, then $P_I = 72000$.

Compute the phase of ionospheric delay

$$X_I = \frac{2\pi(t-50400)}{P_I} \quad (3.13)$$

Compute the slant factor (ionospheric mapping function)

$$F = \left[1 - \left(\frac{R_E}{R_E+h}\cos(E)\right)^2\right]^{-\frac{1}{2}} \quad (3.14)$$

Compute the ionospheric time delay

$$I_I = \{[5 \times 10^{-9} + A_I \cos X_I] \times F\}, \ |X_I| < \frac{\pi}{2} \quad (3.15)$$

Or

$$I_I = \{5 \times 10^{-9} \times F \ |X_I| \geq \frac{\pi}{2}$$

The delay I_I is given in seconds and is referred to the GPS L1 or Beidou B1 frequencies. Although this algorithm is provided to estimate the ionospheric delay in the GPS L1 or Beidou B1 signals, it can also be used to estimate the ionospheric time delay in other frequency signals or for the Glonass and Galileo signals, as well. Indeed, taking into account that the ionospheric delay is inversely proportional to the square of the signal frequency, the delay for any GNSS signal transmitted on frequency f_k is given by

$$I_k = \left(\frac{f_I}{f_k}\right) I_I \quad (3.16)$$

3.3.2 BeiDou model

This model is equivalent to Klobuchar, but it is designed for BeiDou system. The only differences with Klobuchar are that the layer is at 375 km (25 km higher) and that it uses its own model parameters, generated from monitoring stations in China, which are updated

every two hours. These are also broadcasted through the navigation message with the labels "BDSA" and "BDSB" since RINEX version 3.02.

It is stated that BeiDou model outperforms the Klobuchar model for northern hemisphere users in the Asia-Pacific region but exhibits a degraded performance outside this area (Cheng, 2011).

BeiDou system uses eight parameters-Klobuchar model for correcting the ionospheric delay for single frequency users. According to; (Zhao et al., 2014) & (Prasad and Sarma, 2004) and (Sharma and Galav, 2011), the zenith ionospheric delay can be calculated as follows;

$$I_z(t)=\begin{Bmatrix} \{5\times10^{-9} & |t-50400| \geq \frac{\pi}{2} \\ \left[5\times10^{-9}+A_2\cos(\frac{2\pi(t-50400)}{A_4})\right] & \end{Bmatrix}, |t-50400| < \frac{A_4}{4} \qquad (3.17)$$

Where;

Iz is the zenith ionospheric delay for signal frequency B_1 (seconds).

t is time of intersection between the line of receiver to satellite and the ionosphere (in the range of 0–86400) in seconds.

A_2 is the amplitude of the cosine curve on the day calculated by α_n coefficients

A_4 is the period of a cosine curve calculated using the coefficients β_n (seconds)

$$.A_2 = \sum_{n=0}^{3} \chi_n (\Phi m)^n \qquad (3.18)$$

If A_2=0, $A_2 < 0$

$A_4$is the period of a cosine curve calculated using the coefficients β_n (seconds).

$$A_4 = \begin{cases} 7200 & A_4 < 172{,}800 \\ 172{,}800 & A_4 \geq 172{,}800 \\ \sum_{n=0}^{3} \beta_n (\Phi m)^n & 172{,}800 > A_4 \geq 172{,}800 \end{cases} \qquad (3.19)$$

Where,

Φm is the latitude of puncture point (radians).

Φm and λ_m can be calculated as follows:

$$\Phi_m = \arcsin(\sin\varphi_u \cos\psi + \cos\varphi_u \sin\psi \cos A) \qquad (3.20)$$

$$\lambda_m = \lambda_u + \arcsin(\frac{\sin\psi \sin A}{\cos\phi m}) \qquad (3.21)$$

Where,

φ_u is the user geographic latitude (radians).

λ_u is the user geographic longitude (radians).

A is satellite azimuth (radians).

Ψ is geocentric opening angle between user and puncture (radians) which is calculated as ψ =

$$\frac{\pi}{2} - E - \arcsin\left(\frac{R_E}{R_E+h}\cos(E)\right) \qquad (3.\ 22)$$

Where,

R is the radius of the Earth (6,378 km).

E is satellite elevation angle (radians).

h is the height of the ionosphere monolayer (375) km.

Iz (t) can be converted to I_B (t) through

CHAPTER FOUR

DATA AND METHODS

4.1 Data

Study Area and Data Collection:

The study was conducted over the Bahir Dar region in the Amhara region of Ethiopia. Bahir Dar is located in the northern part of the country and is known to experience significant ionospheric activity due to its proximity to the equatorial region.

Table 4.1: Station of study area

Station name	Station code	latitude	Longitude
Bahird Dar	Bdmt	11.5°	37.5°

The data used in this study consisted of:

- GNSS observation data (in RINEX format) collected from a permanent GNSS receiver located in Bahir Dar, Ethiopia, for the entire year of 2015.
- The observation and navigation files of this station is used as an input for gLAB estimation

4.2 Methods

Data Processing using gLAB Software:

The gLAB software suite, developed by the European Space Agency (ESA), was used to process the GNSS data collected over Bahir Dar, Ethiopia, in 2015. The gLAB software is a comprehensive GNSS data analysis tool that can be used for positioning, navigation, and ionosphere modeling.

The data processing was carried out in three scenarios:

Scenario 1 (No Correction):

The GNSS data was processed without any ionospheric correction applied, to establish a baseline for the positioning errors on SPP template of gLAB software with same epoch of observation, and navigation input data.

Scenario 2 (Klobuchar Correction (GPS) :

The Klobuchar ionospheric correction Klobuchar model, which is the standard ionospheric correction method used in the GPS system, was applied to the GNSS same epoch of navigation, and observation input data using the gLAB software on SPP template.

Scenario 3 (Klobuchar Correction (BeiDou**)):**

The Klobuchar ionospheric correction BeiDou model, which is the standard ionospheric correction method used in the BeiDou system, was applied to the GNSS same epoch of navigation, and observation input data using the gLAB software on SPP template.

For all scenarios, the following steps were performed:

1. Download GNSS data of RINEX from UNAVCO'S Data Archive.
2. Preprocessing of the RINEX observation and navigation data files.
3. Application of the necessary corrections, such as satellite clock, satellite ephemeris, ionospheric, and tropospheric corrections.
4. Calculation of the user position using a least-squares algorithm.
5. Comparison of the estimated user position with the known reference coordinates of the GNSS receiver.
6. The position data out put in a form of KLM file and SP3 are used to plot the x-position error (East error), y-position error (North error), and z-position error (up error) for every day we have considered.
7. Calculate maximum horizontal and vertical daily position error by using

   Position error=commuted position value – reference position (priori position)

   $\Delta X_i = X_c - X_r$,$\Delta Y_i = Y_c - Y_r$ and$\Delta Z_i = Z_c - Z_r$. 4. 1

   Maximum horizontal positioning error commutation:

   Maximum horizontal positioning error=$\sqrt{\frac{1}{n}\sum_{i=1}^{n}[(\Delta X_i)^2 + (\Delta Y_i)^2]}$ 4. 2

   Vertical position error commutation:

   Maximum vertical positioning error=$\sqrt{\frac{1}{n}\sum_{i=1}^{n}[(\Delta Z_i)^2]}$ 4. 3
8. Calculating maximum absolute position error between Klobuchar and BeiDou model by using equation of;

   Absolute error = Measured value – corrected value 4. 4
9. RMSE b/n measured value and corrected value between Klobuchar and BeiDou model by using equation of ;

   RMSE= $\sqrt{\frac{1}{n}\sum_{i=1}^{n}(measuredvalue - correctedvalue)^2}$ 4. 5

Performance Evaluation Metrics:

The positioning accuracy was evaluated using the following metrics:

1. Maximum horizontal positioning error (maximum error of East and North)
2. Maximum vertical positioning error (maximum up error)
3. Daily, monthly and seasonal position estimation

CHAPTER FIVE

RESULTS AND DISCUSSIONS

5.1 Daily positioning error commutation

Figures 5.1 through showcase the daily East, North, and up positioning error commutation by various implemented without ionospheric model correction and correction models. Corrections to these positioning error were determined using Klobuchar and BeiDou model adjustments.

On 01 April, around 12hr, the up positioning error scored positioning error of 33m, but on this time East and North positioning error have minimum value. The error by gLAB software analysis without ionospheric correction model registered, vertically 33m, around 7m towards East and, 7.5m towards North. The maximum horizontal positioning error yields 10.3m and spearing maximum vertical positioning error 33m.

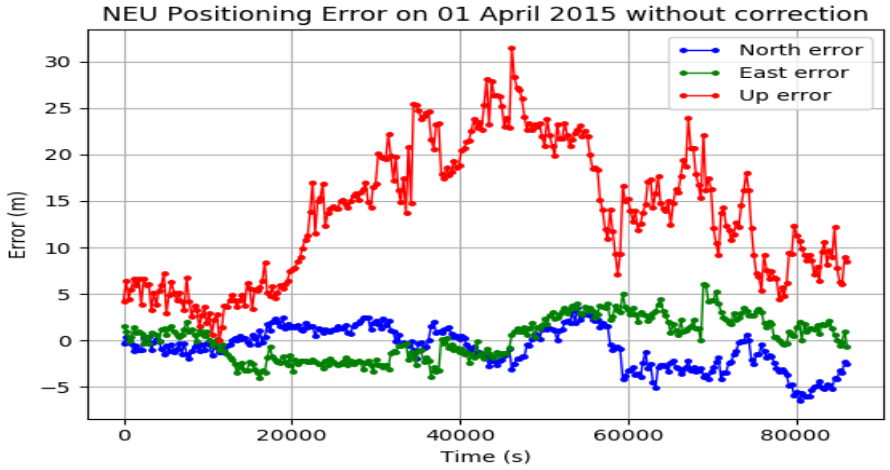

***Figure 5.1**: NEU positioning error uncorrected on 01 April 2015 over Bahir Dar*

Figures 5.2 and 5.3 through showcase the daily East, North, and up positioning error by various implemented with ionospheric correction models. Corrections to these positioning error were determined using Klobuchar and BeiDou model adjustments.

On 01 April, The error by gLAB software analysis Klobuchar (GPS) ionospheric correction model registered, vertically 18m, around 4.5m towards East and, 7m towards North. The maximum horizontal positioning error yields 8.3m and spearing maximum vertical positioning error 18m.

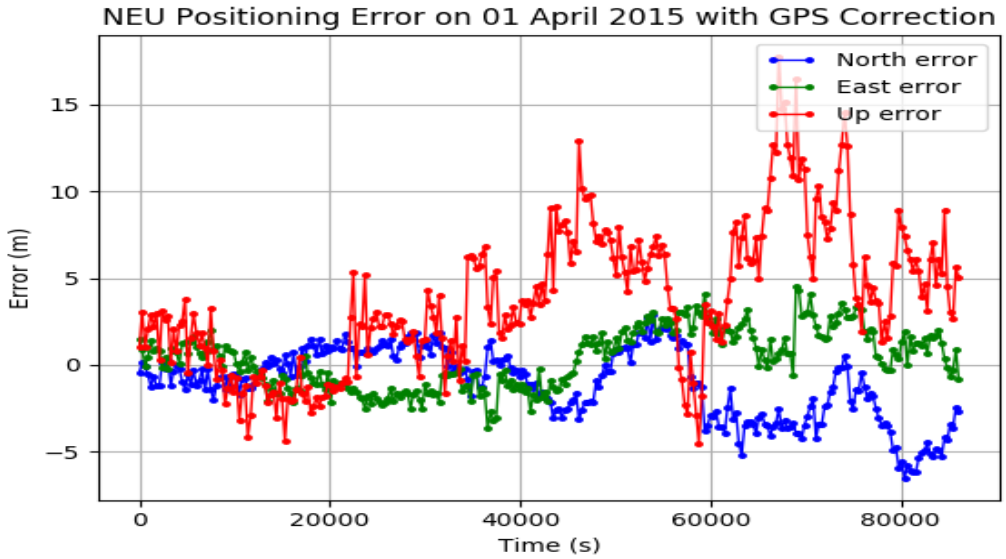

Figure 5.2: *NEU positioning error uncorrected, Klobuchar (GPS) model correction on 01 April 2015 over Bahir Dar*

On 01 April, The error by gLAB software analysis with Klobuchar (BeiDou) ionospheric correction model registered, vertically 28m, around 6m towards East and, 6.8m towards North. The maximum horizontal positioning error yields 9.06m and spearing maximum vertical positioning error 28m.

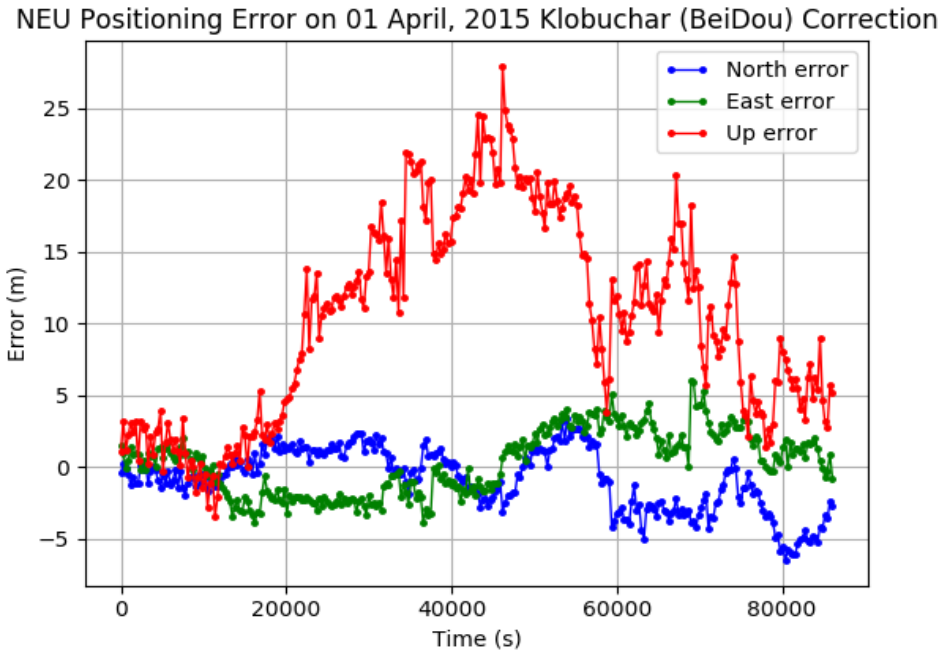

Figure 5.3: *NEU positioning error BeiDou model correction on 01 April 2015 over Bahir Dar*

Table 5.1: horizontal and vertical maximum position error

Ionospheric model	01 April 2015	
	Maximum horizontal positioning error	Maximum vertical positioning error
Without ionospheric correction model	10.3m	33m
Klobuchar(GPS) ionospheric correction model	8.322m	18m
Klobuchar(BeiDou) ionospheric correction model	9.07m	28m

The maximum errors in the y-direction can be attributed to various factors, including the geometry of the satellite constellation and the specific dynamics of the ionosphere affecting signals from certain angles. The y-direction may also be more susceptible to multipath effects in certain environments, such as urban areas or regions with complex terrain. These factors can lead to greater discrepancies in positioning error along that axis. These fluctuations likely stem from the diverse ionospheric dynamics at play, including daily geomagnetic activities that influence the accuracy of positioning error. The detailed analysis of the daily positioning error reveals a nuanced picture of the model's effectiveness in correcting positional discrepancies. By surpassing the performance of both the Klobuchar (GPS)-Klobuchar (BeiDou) model correction and uncorrected positions, the model demonstrates its robustness in providing accurate and reliable error on a day-to-day basis. The observed variations in positioning error values among different days underscore the intricate interplay between ionospheric dynamics and the accuracy of positioning error analysis. These fluctuations suggest a complex relationship between daily geomagnetic activities and the precision of positional corrections, highlighting the need for further investigation into these dynamic factors. At morning and evening time error almost zero by the low ionospheric effect like electron density.

5.2 Daily position estimation fluctuation

The absolute errors between the uncorrected positions and those corrected by Klobuchar model and BeiDou models were computed for each day of the month April in 2015.

Absolute error between the uncorrected and model positions along the x-axis was approximately 0.03m, while the Klobuchar (GPS) model correction yielded 0.04m. Similarly, for the y-axis, the BeiDou model's absolute error was 0.02m, with GPS showing about 0.03m. Additionally, the z-axis estimation error resulted in an absolute error of 0.004m, whereas Klobuchar model registered 0.01m.

These results suggest that on 01 April, the Klobuchar (GPS) model outperformed BeiDou correction in position estimation.

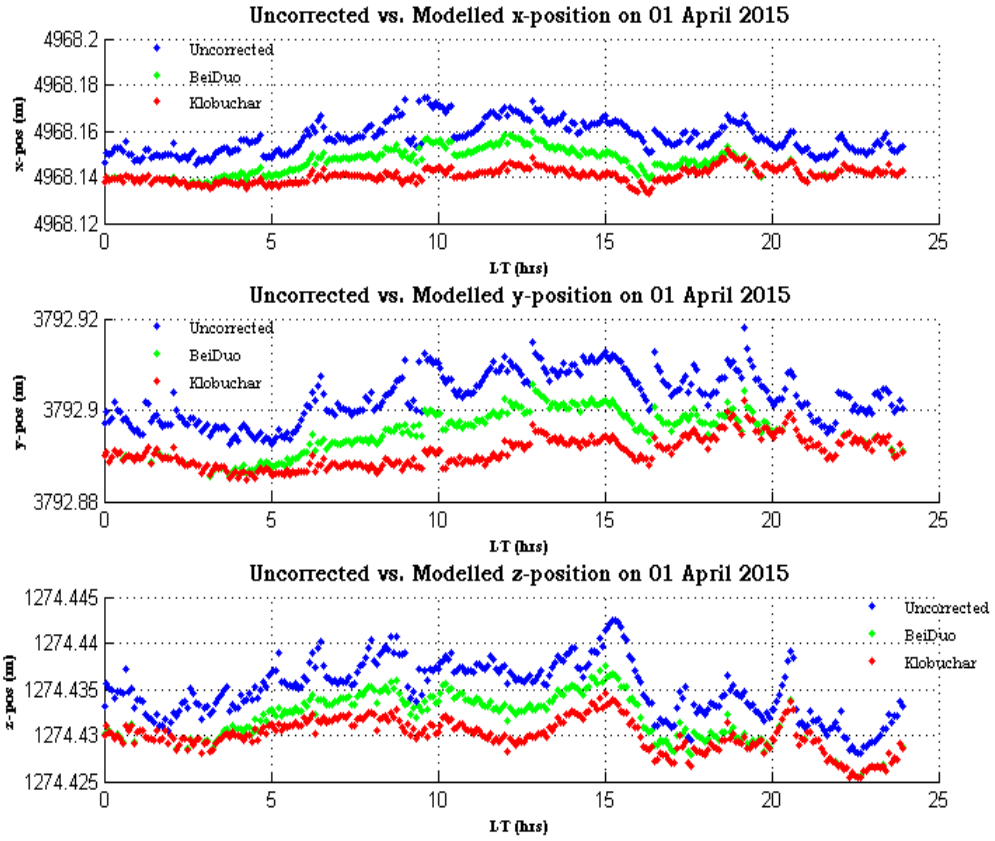

Figure 5.4: *x-y-z position estimation using uncorrected, Klobuchar model and BeiDou model correction on 01 April 2015 over Bahir Dar*

In Figure 5.5, the x-y-z position estimation for April 2, 2015, above Bahir Dar, Ethiopia, is illustrated. The absolute errors between the Klobuchar (GPS) model correction and the BeiDou model correction measure 0.04m and 0.03m along the x-axis, 0.02m and 0.015m along the y-axis, and 0.01m and 0.005m along the z-axis at approximately 10LT.

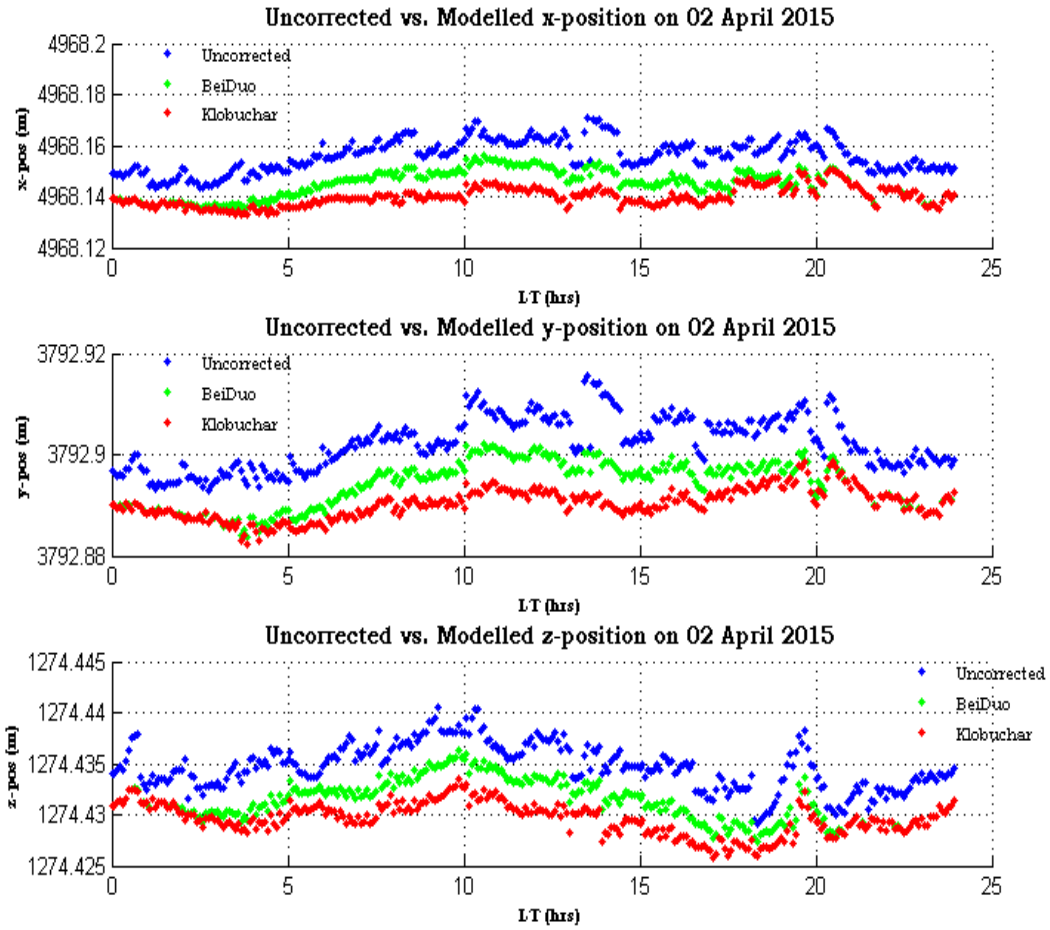

Figure 5.5: *x-y-z position estimation using uncorrected, Klobuchar model and BeiDou model correction on 02 April 2015 over Bahir Dar*

Figures 5.6 provide compelling insights into the daily position estimations, showcasing the superior performance of the model in comparison to both the Klobuchar (GPS)-based correction model and the uncorrected positions. The consistent outperformance of the Klobuchar (GPS) model correction on a daily basis signifies its reliability and accuracy in predicting positional adjustments. Moreover, the presence of varying absolute error values across different days underlines the dynamic nature of these estimations. These fluctuations likely stem from the diverse ionospheric dynamics at play, including daily geomagnetic activities that influence the accuracy of position estimations.

The detailed analysis of the daily position estimations reveals a nuanced picture of the model's effectiveness in correcting positional discrepancies.

By surpassing the performance of both the Klobuchar (GPS) model based correction and uncorrected positions, the model demonstrates its robustness in providing accurate and

reliable estimations on a day-to-day basis. The observed variations in absolute error values among different days underscore the intricate interplay between ionospheric dynamics and the accuracy of position estimations. These fluctuations suggest a complex relationship between daily geomagnetic activities and the precision of positional corrections, highlighting the need for further investigation into these dynamic factors.

The discrepancies in absolute error values across varying days not only emphasize the importance of considering daily ionospheric variations but also point towards the potential impact of daily geomagnetic activities on position estimation accuracy. The Klobuchar (GPS) model correction consistent outperformance underscores its capability to account for these dynamic factors and provide reliable estimations in the face of changing environmental conditions. Understanding and accounting for these daily variations in ionospheric dynamics and geomagnetic activities are crucial for enhancing the precision and reliability of position estimations, thereby advancing our comprehension of the complexities involved in satellite-based positioning systems.

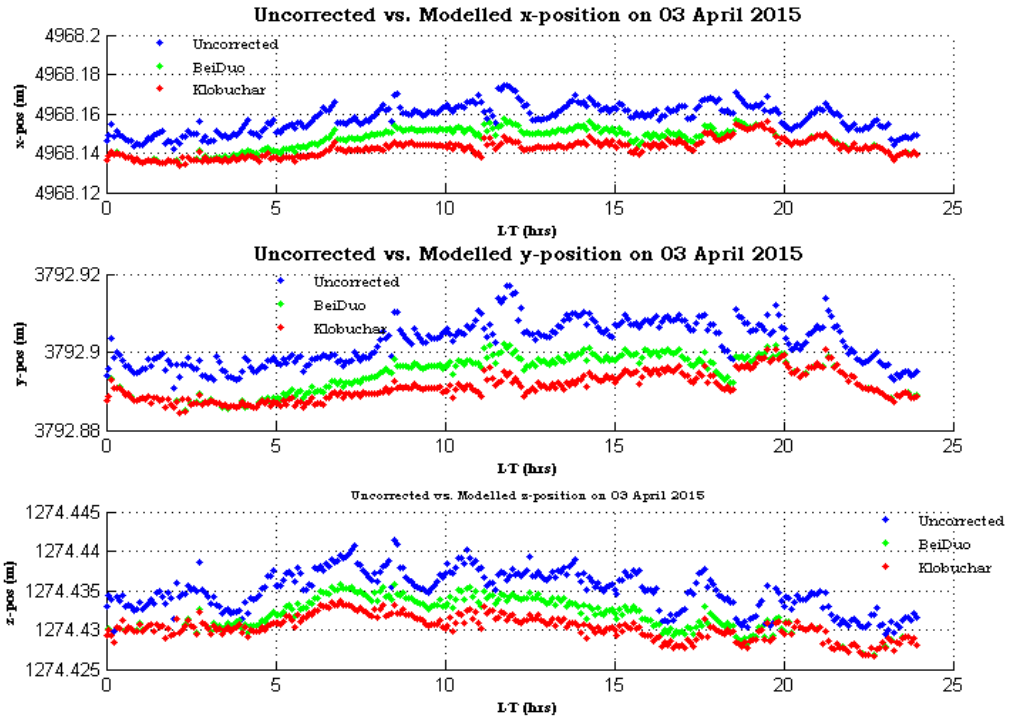

Figure 5.6: *x-y-z position estimation using uncorrected, Klobuchar model and BeiDou model correction on 03 April 2015 over Bahir Dar*

The discrepancies in absolute error values across varying days not only emphasize the importance of considering daily ionospheric variations but also point towards the potential impact of daily geomagnetic activities on position estimation accuracy. The model's

consistent outperformance underscores its capability to account for these dynamic factors and provide reliable estimations in the face of changing environmental conditions. Understanding and accounting for these daily variations in ionospheric dynamics and geomagnetic activities are crucial for enhancing the precision and reliability of position estimations, thereby advancing our comprehension of the complexities involved in satellite-based positioning systems.

5.3 The monthly fluctuations in position estimation

Figures 5.7 to 5.9 display the monthly fluctuations in position estimation along the x, y, and z axes utilizing Klobuchar model based and BeiDou model corrections. The corresponding absolute errors and root mean square errors for these monthly estimations are detailed in Tables 5.2 and 5.3. Analysis of these figures and tables reveals that the average absolute errors were 0.0125m for the BeiDou model and 0.0147m for Klobuchar (GPS) model in x-positioning, 0.0092 for the BeiDou model and 0.0109 for Klobuchar (GPS) model in y-positioning, and 0.0038m for the BeiDou model and 0.0045m for Klobuchar (GPS) model in z-positioning. Similarly, the average root mean square errors were 0.0147m for the BeiDou model and 0.0125m for Klobuchar (GPS) model in the x-direction, 0.0109m for the BeiDou model and 0.0092 for Klobuchar (GPS) model in the y-direction, and 0.0045m for the BeiDou model and 0.0038m for Klobuchar (GPS) model in the z-direction. These averages indicate that the model consistently outperformed in monthly estimations.

Despite the Klobuchar (GPS) model correction superior performance on average, a closer examination of the tabulated data reveals clear variations in month-to-month estimations. Notably, the minimum absolute errors and root mean square errors were observed around June and December of the year 2015. These findings suggest that while the model generally excels in monthly estimation, specific months exhibit lower errors, indicating potential seasonal or environmental influences on the accuracy of position estimations during those periods. Monthly variations in ionospheric corrections in position estimation can be attributed to several factors. Firstly, changes in solar activity play a significant role. Solar flares, sunspots, and variations in solar radiation can impact the ionosphere, leading to fluctuations in ionization levels. During periods of heightened solar activity, increased ionization can result in signal delays and errors in position estimation as GPS signals traverse through this layer.

Geomagnetic storms also contribute to monthly variations in ionospheric corrections. These storms, caused by fluctuations in the Earth's magnetic field due to interactions with solar

wind, can disrupt the ionosphere. The irregularities in electron density distribution during geomagnetic storms can introduce fluctuations in signal propagation, affecting the accuracy of position calculations.

Seasonal changes influence the ionosphere as well. Variations in solar incidence angle and the Earth's orientation throughout the year lead to seasonal fluctuations in the electron density distribution of the ionosphere. These variations impact the speed and propagation of GPS signals, introducing biases in position estimations that need to be accounted for to ensure accurate results.

Additionally, factors such as changes in magnetic declination and ionospheric weather conditions contribute to monthly variations in ionospheric corrections. Magnetic declination alterations affect the behavior of charged particles in the ionosphere, influencing signal refraction and delays. Ionospheric weather events, including storms, disturbances, and irregularities, can cause rapid fluctuations in electron density that disrupt GPS signal propagation, leading to unpredictable errors in position estimations. Monitoring and adjusting for these diverse factors are essential for improving the accuracy and reliability of position calculations in satellite-based navigation systems, particularly in the presence of dynamic ionospheric conditions.

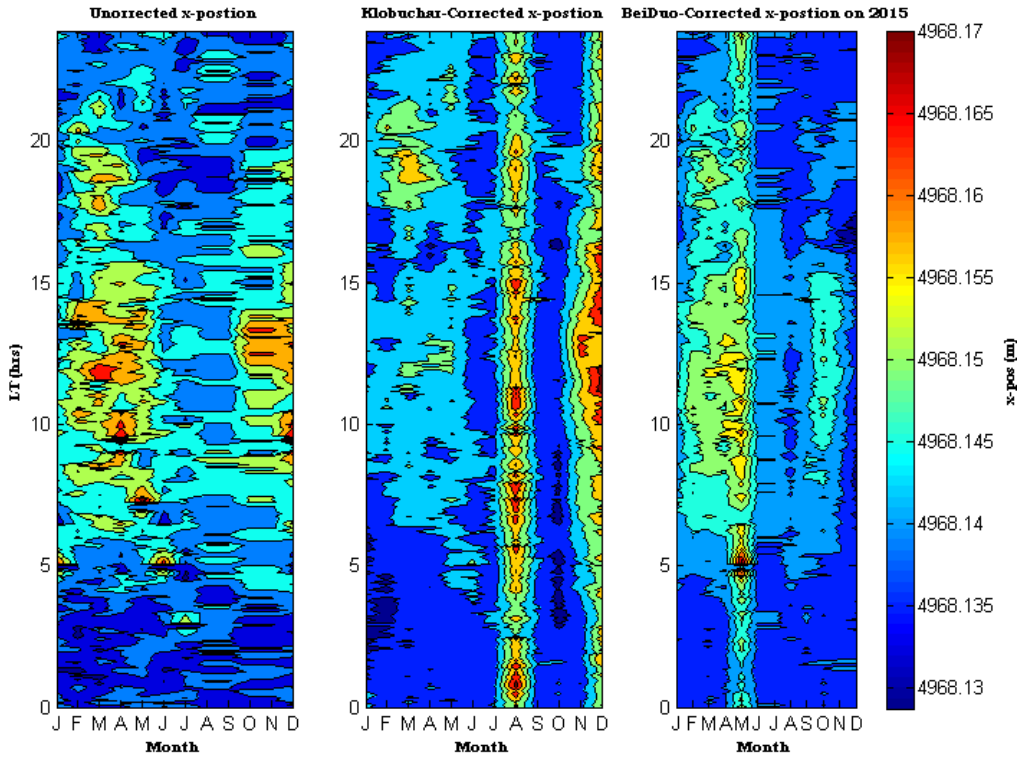

Figure 5.7: *Monthly fluctuations in position estimation along the x-direction*

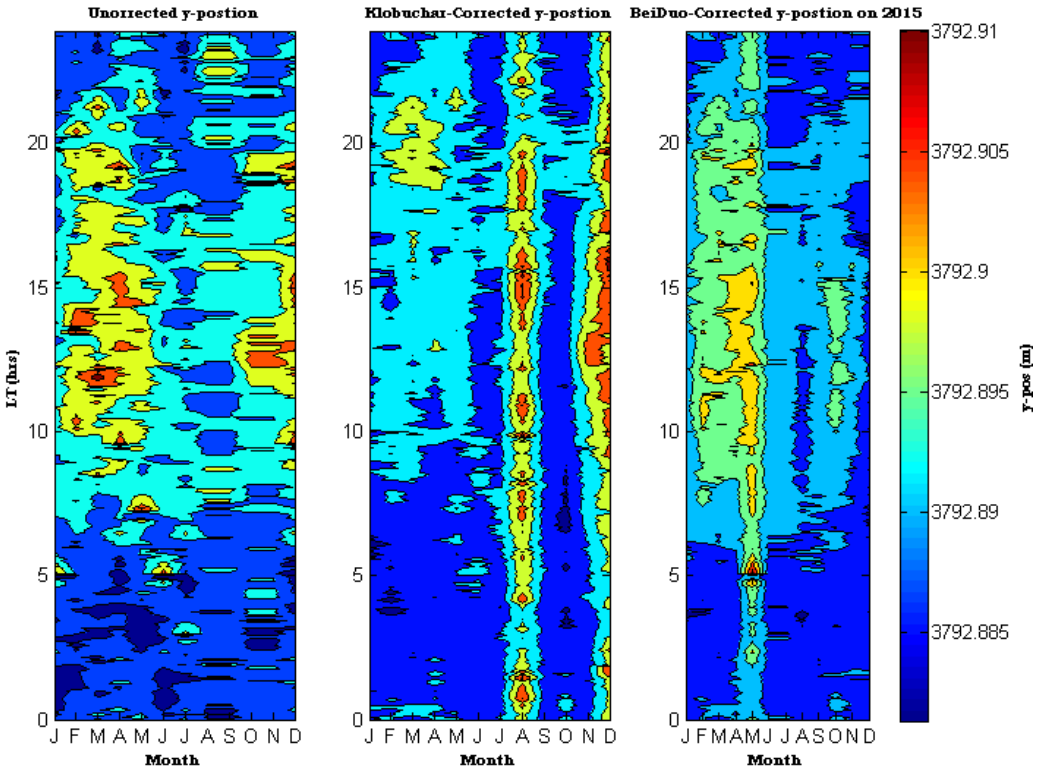

Figure 5.8: *Monthly fluctuations in position estimation along the y-direction*

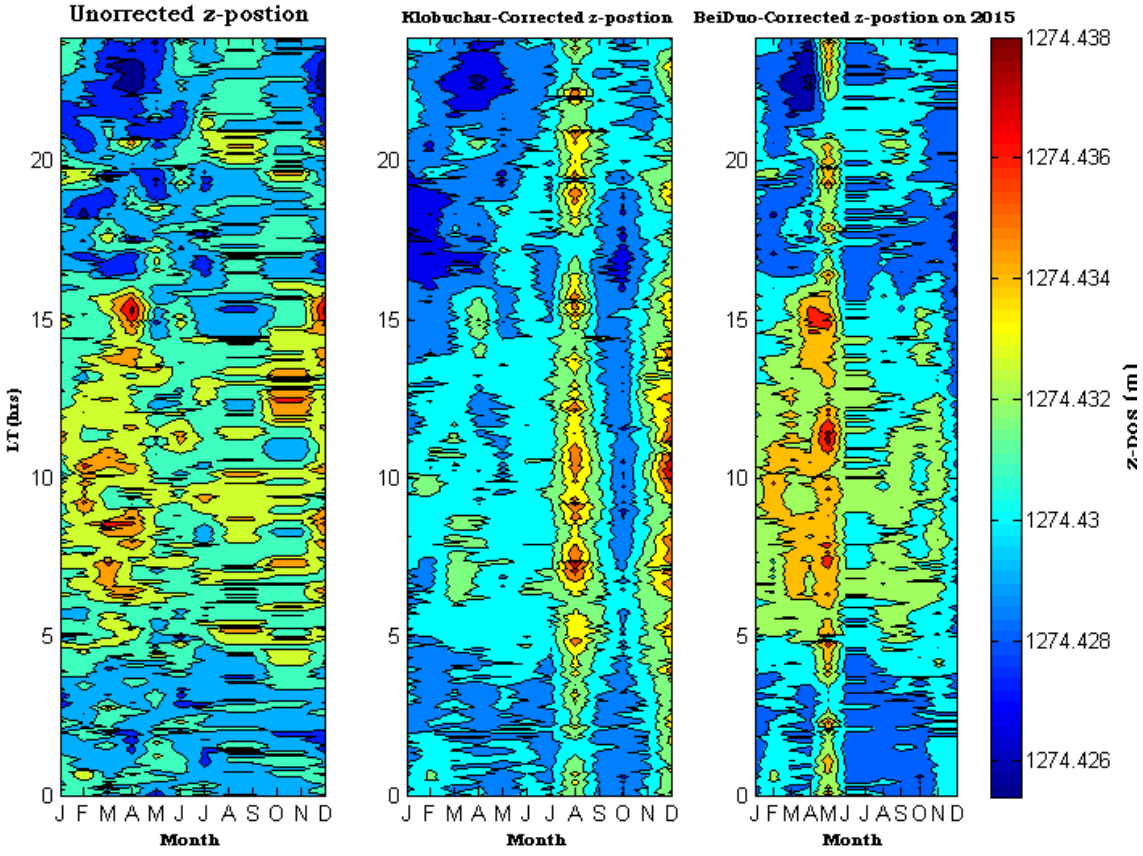

Figure 5. 9: *Monthly fluctuations in position estimation along the z-direction*

Table 5. 2: Monthly Fluctuations in Absolute Error.

Month	Maximum Absolute Error					
	X-position (in meter)		Y-position (in meter)		Z-position (in meter)	
	Klobuchar (GPS) model corrected	BeiDou model corrected	Klobuchar (GPS) model corrected	BeiDou model corrected	Klobuchar (GPS) model corrected	BeiDou model corrected
January	0.0367	0.0293	0.0256	0.0217	0.0108	0.0075
February	0.0296	0.0199	0.0235	0.0151	0.0090	0.0066
March	0.0293	0.0195	0.0232	0.0159	0.0088	0.0069
April	0.0347	0.0223	0.0230	0.0143	0.0091	0.0064
May	0.0311	0.0219	0.0222	0.0155	0.0078	0.0055
June	0.0259	0.0329	0.0181	0.0248	0.0072	0.0077
July	0.0241	0.0226	0.0162	0.0161	0.0068	0.0063
August	0.0136	0.0270	0.0119	0.0203	0.0062	0.0091
September	0.0226	0.0212	0.0188	0.0187	0.0066	0.0066
October	0.0338	0.0253	0.0261	0.0180	0.0129	0.0098
November	0.0201	0.0291	0.0177	0.0205	0.0064	0.0100
December	0.0232	0.0404	0.0164	0.0300	0.0079	0.0148
Average	**0.0271**	**0.02595**	**0.0202**	**0.0192**	**0.0083**	**0.0081**

Table 5. 3: Monthly Fluctuations in Root Mean Square Error.

Month	Root Mean Square Error (RMSE)					
	X-position (in meter)		Y-position (in meter)		Z-position (in meter)	
	Klobuchar (GPS) model corrected	BeiDou model corrected	Klobuchar (GPS) model corrected	BeiDou model corrected	Klobuchar (GPS) model corrected	BeiDou model corrected
January	0.0154	0.0131	0.0112	0.0096	0.0054	0.0037
February	0.0169	0.0116	0.0126	0.0086	0.0053	0.0035
March	0.0159	0.0117	0.0117	0.0086	0.0049	0.0035
April	0.0176	0.0119	0.0129	0.0085	0.0053	0.0036
May	0.0155	0.0069	0.0114	0.0053	0.0043	0.0025
June	0.0147	0.0133	0.0108	0.0096	0.0041	0.0042
July	0.0140	0.0123	0.0103	0.0090	0.0039	0.0037
August	0.0051	0.0147	0.0046	0.0115	0.0020	0.0041
September	0.0149	0.0127	0.0114	0.0097	0.0042	0.0039
October	0.0198	0.0137	0.0144	0.0100	0.0064	0.0046
November	0.0124	0.0160	0.0093	0.0111	0.0037	0.0044
December	0.0076	0.0217	0.0056	0.0160	0.0026	0.0063
Average	**0.0147**	**0.0125**	**0.0109**	**0.0092**	**0.0045**	**0.0038**

5.4 Seasonal Positioning Estimation

Figures 5.10 to 5.12 showcase the seasonal variations in positioning estimation along the x, y, and z axes using Klobuchar model and BeiDou model based corrections. Throughout these analyses, the Klobuchar (GPS) model consistently demonstrated superior performance over BeiDou model based corrections. Notably, a distinct seasonal trend emerged in the estimation process, with errors peaking during the March and September equinoxes and decreasing during the solstice seasons. These fluctuations in position estimation accuracy across seasons suggest a correlation with neutral wind dynamics, particularly the ion accumulation dynamics during equinoctial seasons compared to solstice seasons. The accumulation of ions in the ionosphere during specific periods could introduce significant errors in determining positioning along the x, y, and z directions.

In Figure 5.11, the average absolute and root mean square errors in position estimation are depicted. The blue bar shows uncorrected, brown bars signify errors associated with Klobuchar model corrections, while the green bars represent errors stemming from BeiDou model based corrections along the x, y, and z directions. Noteworthy is the observation of minimum errors in x-direction estimations, with maximum errors evident in the y-direction estimations. However, the overall trend reinforced that the model consistently outperformed Klobuchar model corrections in position estimation. These findings underscore the reliability and accuracy of the Klobuchar (GPS) model based approach in enhancing positioning estimations compared to traditional BeiDou model corrections. The comprehensive analysis of seasonal variations in positioning estimation not only highlights the model's superior performance over BeiDou model correction but also sheds light on the impact of seasonal changes on positioning accuracy. The magnified errors during the equinoxes and reduced errors during solstice seasons point towards a complex interplay between neutral wind dynamics and ion accumulation dynamics in the ionosphere. Understanding these seasonal variations is crucial for refining positioning technologies and ensuring accurate location determinations along the x, y, and z axes, thus improving the overall reliability of Klobuchar (GPS) model based systems in diverse environmental conditions.

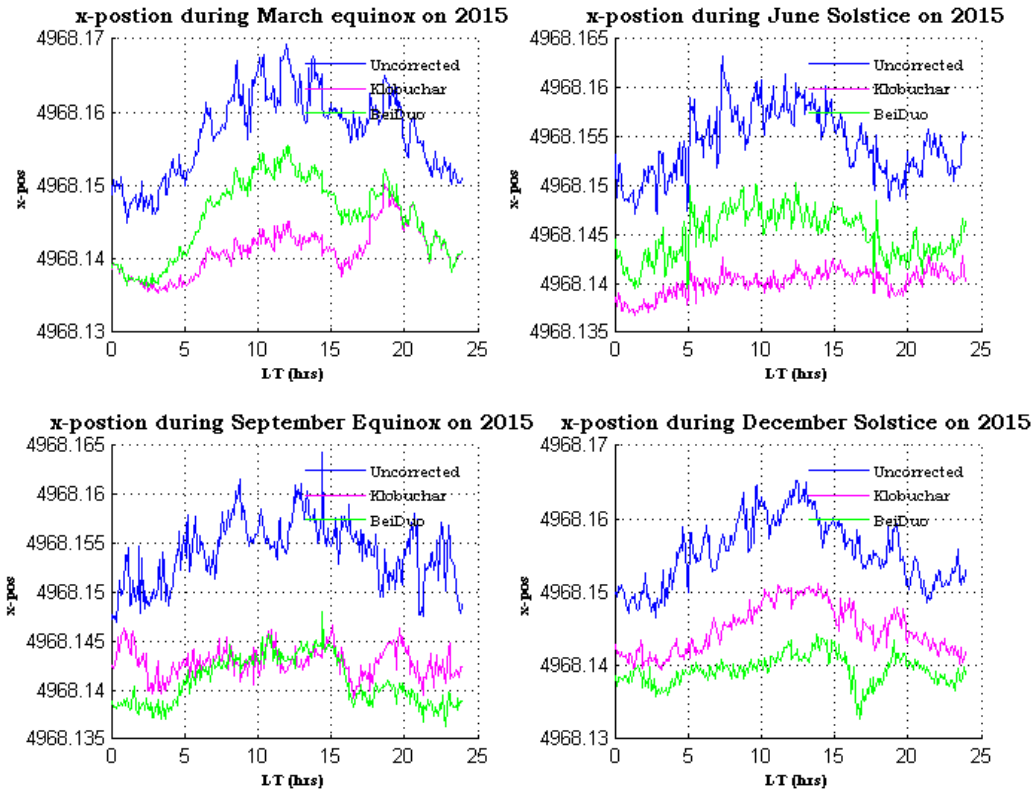

Figure 5. 10: *Seasonal Positioning Estimation along the x-direction*

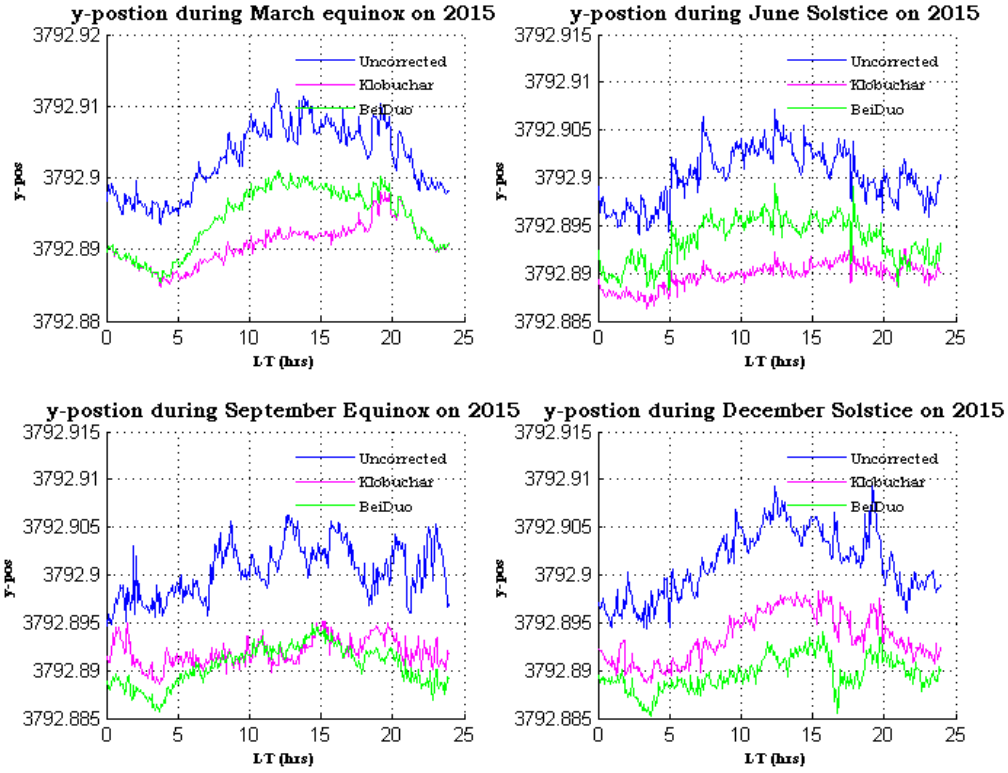

Figure 5.11: *Seasonal Positioning Estimation along the y-direction*

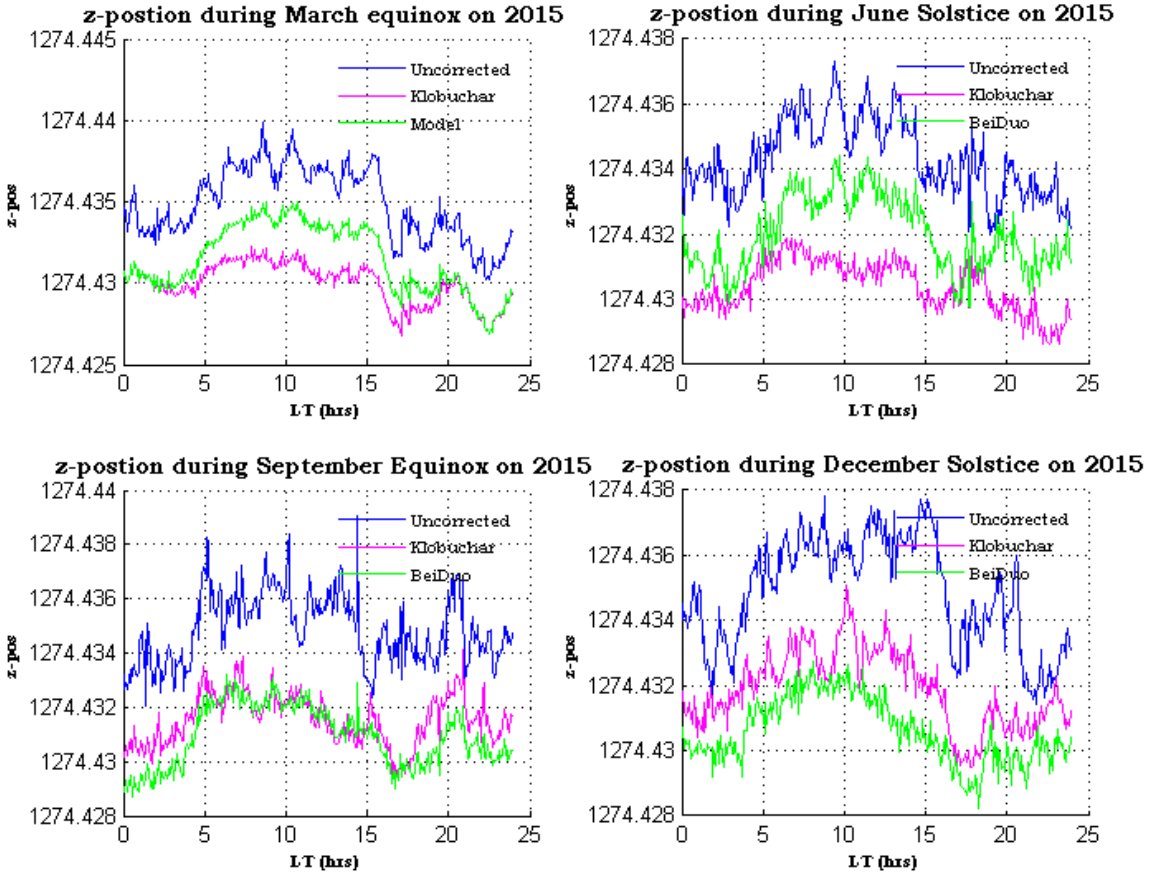

Figure 5. 12: *Seasonal Positioning Estimation along the z-direction*

CHAPTER SIX

CONCLUSIONS AND RECOMMENDATIONS

6.1 Conclusions

From the detailed analysis of daily and monthly fluctuations in position estimation using Klobuchar model and BeiDou model corrections, several key conclusions can be drawn. Figures 5.1 to 5.3 represents the daily fluctuations in position error reveal that the Klobuchar (GPS) model consistently outperformed BeiDou model correction on 01 April, indicating its superior accuracy in predicting positional adjustments. Figures 5.4 to 5.6 illustrate the daily x, y, and z positions estimated by various models, showcasing how corrections using Klobuchar model and BeiDou models significantly improved position accuracy. The fluctuating absolute error values across different days highlight the dynamic nature of these estimations, influenced by ionospheric dynamics and daily geomagnetic activities.

Moving on to monthly position estimations, the fluctuations depicted in Figures 5.7 to 5.9 indicate that, on average, the Klobuchar (GPS) model's consistently outperformed over BeiDou model in x, y, and z positioning. Despite the BeiDou model's overall superiority, variations in absolute and root mean square errors were observed month-to-month, with lower errors typically around June and December, suggesting seasonal or environmental influences on accuracy. Factors such as solar activity, geomagnetic storms, seasonal changes, magnetic declination alterations, and ionospheric weather conditions contribute to monthly variations in ionospheric corrections, requiring careful monitoring and adjustment for precise position calculations.

Regarding seasonal position estimations, the variations in positioning accuracy shown in Figures 5.10 to 5.12 highlighted a distinct trend with errors peaking during equinoxes and decreasing during solstice seasons. The Klobuchar (GPS) model's consistently demonstrated superior performance over BeiDou model corrections across seasons, with errors in positioning accuracy correlating with neutral wind dynamics and ion accumulation dynamics during specific periods. Understanding seasonal variations in positioning accuracy is crucial for refining positioning technologies and ensuring accurate location determinations, particularly in diverse environmental conditions.

The study's findings emphasize the importance of considering daily, monthly, and seasonal fluctuations in position estimation accuracy, highlighting the intricate interplay between ionospheric dynamics, geomagnetic activities, and environmental factors. The consistent outperformance of the Klobuchar (GPS) model over BeiDou model corrections underscores

its reliability in providing accurate estimations, with implications for improving the overall precision and reliability of satellite-based positioning systems. Continued research into these dynamic factors is vital for advancing our understanding of satellite-based navigation and enhancing the effectiveness of position estimation technologies in various environmental conditions.

6.2 Recommendations

While the thesis provides valuable insights into the daily, monthly, and seasonal fluctuations in position estimation accuracy using Klobuchar model and BeiDou model corrections, several limitations should be acknowledged.

Recommendations for Future Research:

Explore Alternative Correction Models: Investigating alternative correction models and algorithms beyond the BeiDou and Klobuchar models could offer insights into improving accuracy and reliability in position estimations.

Long-Term Monitoring: Conducting long-term monitoring to capture more extensive datasets could help in identifying trends, patterns, and anomalies in position estimations over extended periods.

Integration of Multi-constellation Systems: Considering the integration of multi-constellation systems (e.g., GPS, Galileo, GLONASS) could enhance the robustness and accuracy of position estimations by leveraging signals from multiple satellite systems.

By addressing these recommendations in future research endeavors, it is possible to further advance our understanding of position estimation accuracy fluctuations and improve the reliability of satellite-based navigation systems in diverse environmental conditions.

.

Bibliography

Abd-Elazeem M., Farah A., Farrag F. (2011): *Assessment study of using online (CSRS) GPS-PPP Service for mapping applications in Egypt*. Journal of Geodetic Science, vol. **1**, no. 3, pp. 233–239. https://doi.org/10.2478/v10156-011-0001-3.

Addisie Nuru. (2019). Spatio-temporal variability of the horizontal component of space source earth's magnetic field.

Aragaw Misganaw (2017). Solar activity and geomagnetic storm effects on gps ionospheric tec over ethiopia,

Elbert (2004). the Satellite Communication Applications Handbook, Second Edi. London: Artech House, , pp. 7–14.

Brekke, A. (2013). Physics of the upper polar atmosphere, Springer Science & Business Media.

Russell, R. L. McPherron and R. K. Burton (1974). Journal of Geophysical Research, 79, 1105-1109.

Chapman, S. (1931). A theory of the ionosphere. *Proceedings of the Royal Society A: Mathematical, Physical and Engineering Sciences*, ***133***(821), 457-475

Cheng and Dang, 2011] Cheng, P. and Dang, Y., 2011. China National Report on Geodesy (2007-2010). Chinese National Committee for IAG, Chinese National Committee for The International Union of Geodesy and Geophysics, Beijing, China.

Davies, K. (1990). Ionospheric radio. *Peter Peregrinus Ltd.*

Deimos Ibanez Segura (2014)). Implementation of GNSS ionospheric models in gLAB, Universitat Politecnica de Catalunya, pp 12-20

El Shouny A., Miky Y.(2019) *Accuracy assessment of relative and precise point positioning online GPS processing services*. Journal of Applied Geodesy, vol. **13**, no. 3, , pp. 215–227. https://doi.org/10.1515/jag-2018-0046.

Enge, p., and Misra, (1999). special issue: GPS and future of navigation. Proceeding of IEEE, 87, 7-13

Ershad Ali (2021). Global Positioning System (GPS): Definition, Principles, Errors, Applications & DGPS, (2020), University of North Bengal. (pp 3-5)

European GNSS (Galileo) Open Service Signal In Space Interface Control Document (OS SIS ICD), Issue 2.0, European Union, January.

Kumar, G. S. B. Rao, and M. N. V. S. S. Kumar, (1998) "GPS Signal Short-Term Propagation Characteristics Modeling in Urban Areas for Precise Navigation Applications," Positioning, vol. **04**, no. 02, pp. 192–199, 2013.

Gao Y, Liu Z. (2002). Precise ionospheric modeling using regional GPS network data. J Glob Pos Syst. **1**(1), 18–24.

Ghoddousi-Fard R., Dare P.(2006). Online GPS processing services: an initial study. GPS Solutions, vol. **10**, no. 1, pp. 12–20. https://doi.org/10.1007/s10291-005-0147-5.

Goldhirsh and W. J. Vogel, Handbook of Propagation Effects for Vehicular and Personal Mobile Satellite Systems Overview of Experimental and Modeling Results , vol. **021**, no. December. Texas.

Hargreaves, J. K. (1992). The Solar-Terrestrial Environment. Cambridge University Press.

Hernandez-Pajares M., Juan J., Sanz J., Ramos-Bosch P., Rovira-Garcia A., Salazar D., Ventura-Traveset J., Lopez-Echazarreta C., Hein G. (2010): The ESA/UPC GNSS-Lab tool (gLAB): An advanced multipurpose package for GNSS data processing.

Hofmann-Wellenhof B, Lichtenberger H, Collins J. (1992). Global Positioning Systems theory and practice Springer-Verlag Wien, New York

Hunsucker, R. D., and Hargreaves, J. K. (1995). The high latitude Ionosphere and its effect on Radio propagation. Cambridge University Press.

Ioannides, R.T., H.J. Strangeways (2000). Ionosphere-induced errors in GPS range finding using MQP modelling, ray-tracing and Nelder-Mead optimization (2000). Millennium Conference on Antennas and Propagation, AP, vol. **2**, Davos, 404–408

Louis J. Ippolito (2008). Communications Atmospheric Effects, Satellite Link Design. Washington: A John Wiley and Sons, Ltd, pp. 89–82.

Wan A. W. Z. Abidin (2008). "Novel Approach to Determine the Effects of MS Environment using the Portable GPS Receiver with Built-in Antenna," Am. J. Appl. Sci. , vol. **5**, no. 8, pp. 1079–1082,.

Kelley, M.C.; Kotsikopoulos, D.; Beach, T.; Hysell D.; Musman S (1996). *Simultaneous global positioning system and radar observations of equatorial spread F* at. Journal of Geophysical Research., **101**, 2333

Kintner, P. M. III. Minter, C. J., and Hargreaves, J. K. (2007). GPS and ionosphere: A review of issues and solution. **42**(2).

Kintner, P. M., & Ledvina, B. M. (2004). GPS and the ionosphere: A review of the effects of the ionosphere on GPS measurements. Proceedings of the IEEE, ***92***(4), 538-551.

Klobuchar JA, Parkinson BW, Spilker JJ (1996). Ionospheric effects on GPS, in global positioning system: theory and applications. American Institute of Aeronautics and Astronautics, Washington D.C

Klobuchar, J. A. (1988). Ionospheric effects on GPS. In Proceedings of the IEEE Position Location and Navigation Symposium, (pp. 90-95).

Kong J.-M., Park J.-K., Lee C.-G., Lee Y.-W (2010). *Accuracy analysis of online GPS data processing service*. Journal of the Korean Society of Surveying, Geodesy, Photogrammetry Cartography, vol. 28, no. **1**, pp. 13–20.

Hoque and N. Jakowski (2000). "Ionospheric Propagation Effects on GNSS Signals and New Correction Approaches," in Global Navigation Satellite Systems – Signal, Theory and Applications , Germany, pp. 381–394.

Hernandez-Pajares, J.M. Juan, J.Sanz, P. Ramos-Bosch (2014) : An advanced multipurpose package for GNSS data processing. 1Research group of Astronomy and Geomatics, Universitat Politecnica de Catalunya (gAGE/UPC), Barcelona, Spain

Hernandez-Pajares1, J.M. Juan1, J.Sanz1 (2021). An advanced multipurpose package for GNSS data processing. Universitat Politecnica de Catalunya (pp-4)

Matsushita S, Campbell WH (1967).Physics of geomagnetic phenomena, vol **1**. Academic Press, New York

McNamara, L. F. (1991). The ionosphere: communications, surveillance, and direction finding, Krieger publishing company.

Merwe, S. J. V. (2011). Characterization Of The Ionosphere Over South Atlantic Anomaly By Using A Ship Based Dual Frequency Gps Receiver As Aid For Hf Propagation Path Prediction. University of Pretoria South Africa.

Ocalan T.: Accuracy assessment of GPS precise point positioning (PPP) technique using different web-based online services in a forest environment. Šumarski list, 2016, vol. **140**, no. 7–8, pp. 357–367. https://doi.org/10.31298/sl.140.7-8.4.

Reddy C (2002) Study of space weather effects using GPS. In: Proceedings , GPS in Atmospheric Sciences. India International Centre, New Delhi.

Sanz, J., Hernández-Pajares, M., Juan, J. M., & Orús, R. (2013). The new IONEX format for ionospheric data. *GPS Solutions*, ***17***(1), 1-10.

Susnik, j., and Forte, B. (2011). *Analysis of GPS performance in urban environment*. Journal of navigation 64(3), 505-520

Tétreault P., Kouba J., Héroux P., and Legree P.J.G (2005).: *CSRS-PPP*: an internet service for GPS user access to the Canadian Spatial Reference Frame. vol. **59**, no. 1, pp. 17–28.

Vinh, N. X., Van, H. C., & Nguyen, T. D. (2013). *The influence of the ionosphere on GPS positioning accuracy. Journal of Geodesy*, ***87***(6), 485-495.